Infectious Disease Modelling 9 (2024) 569–600

Contents lists available at ScienceDirect

Infectious Disease Modelling

journal homepage: www.keaipublishing.com/idm

Impact of infectious density-induced additional screening and treatment saturation on COVID-19: Modeling and cost-effective optimal control

Sonu Lamba [a], Tanuja Das [a, b], Prashant K. Srivastava [a, *]

[a] Department of Mathematics, Indian Institute of Technology Patna Bihta – 801106, Patna, Bihar, India
[b] Department of Mathematics and Statistics, University of New Brunswick Fredericton, NB, E3B 5A3, Canada

ARTICLE INFO

Article history:
Received 6 October 2023
Received in revised form 18 February 2024
Accepted 11 March 2024
Available online 16 March 2024
Handling Editor: Dr Yiming Shao

Keywords:
COVID-19
IDIAS
Estimation
Prediction
Optimal control
Cost-effectiveness analysis

ABSTRACT

This study introduces a novel *SI2HR* model, where "*I2*" denotes two infectious classes representing asymptomatic and symptomatic infections, aiming to investigate and analyze the cost-effective optimal control measures for managing COVID-19. The model incorporates a novel concept of infectious density-induced additional screening (IDIAS) and accounts for treatment saturation. Furthermore, the model considers the possibility of reinfection and the loss of immunity in individuals who have previously recovered. To validate and calibrate the proposed model, real data from November–December 2022 in Hong Kong are utilized. The estimated parameters obtained from this calibration process are valuable for prediction purposes and facilitate further numerical simulations. An analysis of the model reveals that delays in screening, treatment, and quarantine contribute to an increase in the basic reproduction number R_0, indicating a tendency towards endemicity. In particular, from the elasticity of R_0, we deduce that normalized sensitivity indices of baseline screening rate (θ), quarantine rates (γ, α_s), and treatment rate (α) are negative, which shows that delaying any of these may cause huge surge in R_0, ultimately increases the disease burden. Further, by the contour plots, we note the two-parameter behavior of the infectives (both symptomatic and asymptomatic). Expanding upon the model analysis, an optimal control problem (OCP) is formulated, incorporating three control measures: precautionary interventions, boosted IDIAS, and boosted treatment. The Pontryagin's maximum principle and the forward-backward sweep method are employed to solve the OCP. The numerical simulations highlight that enhanced screening and treatment, coupled with preventive interventions, can effectively contribute to sustainable disease control. However, the cost-effectiveness analysis (CEA) conducted in this study suggests that boosting IDIAS alone is the most economically efficient and cost-effective approach compared to other strategies. The CEA results provide valuable insights into identifying specific strategies based on their cost-efficacy ranking, which can be implemented to maximize impact while minimizing costs. Overall, this research offers significant insights for policymakers and healthcare professionals, providing a framework to optimize control efforts for COVID-19 or similar epidemics in the future.

* Corresponding author.
E-mail address: pksri@iitp.ac.in (P.K. Srivastava).
Peer review under responsibility of KeAi Communications Co., Ltd.

https://doi.org/10.1016/j.idm.2024.03.002

1. Introduction

In epidemiology, many contagious diseases that emerge or re-emerge require quick and targeted repercussions. There is nothing better than immunizing the afflicted populace with some kind of vaccination or treatment; however, it's not always the case. For instance, during the early stages of COVID-19's emergence, pharmaceutical interventions like vaccines and medications were not readily available worldwide. Similarly, when a new disease initially emerges, it's not always possible to access or develop the necessary medicinal resources. As a result, we rely heavily on non-pharmaceutical control mechanisms, including social isolation, masking, testing or screening, and so on. When disease prevalence is higher and reliable swift diagnostic facilities are available, screening as a standalone measure may be effective. Screening for COVID-19 has been crucial in controlling the spread of the virus by identifying individuals who are infected, either through symptoms or testing, and isolating them. It also helps to identify asymptomatic individuals who can unknowingly spread the virus, high-risk individuals for severe illness, and outbreaks. But due to even a minor possibility of false positive test results, screening in low prevalence scenarios may lead to an unwarranted saturation of healthcare resources and disease burden (Wald et al., 1999). Therefore, an efficient and effective screening technique is always useful in counteracting any rapid epidemic in a community.

Almost half a century ago, the World Health Organization (WHO) published a comprehensive report on "Principles and practice of screening for disease" by Wilson and Jungner, popularly known as the *Wilson-Jungner criterion* of disease detection (Maxwell Glover Wilson & Jungner, 1968). Listed below are some of the crux points (Andermann et al., 2008) of that criterion, which became the public health paradigm.

1. There should be a discernible latent/early symptomatic or asymptomatic infectious stage.
2. An apt test should be well-received by the population it is designed for.
3. The project should not be a 'once and for all.' It should continue until the condition persists.
4. The process should be cost-effective as a whole.

Several mathematical modelers have tried incorporating the points of this classic criteria by defining some specific screening rate functions in disease models. For an example, one of the earliest works includes a random screening of the infectious population; this work by Hsieh (Hsieh, 1991) was based on the initial model of HIV dynamics given by May and Anderson (Robert Mccredie May and Roy Malcolm Anderson, 1988). Kim and Milner (Kim & Milner, 1995) extended the work of Hsieh (Hsieh, 1991) by modifying the screening rate function while studying the effect of screening on a disease model with variable infectiousness; the authors took $\sigma(y)/y$ as screening rate per unit time, with active population $y = S + I$. The purpose of taking this kind of screening rate was to partially incorporate the third point (mentioned above) of the WJ criterion. Their argument was that the screening should be directly proportional to the active infectious population (y) and inversely proportional to the non-susceptibility (S/I), which they showed by re-writing the removal term as $\sigma(y)/(1 + S/I)$. If seen from the other perspective, this rate function also incorporates the saturation caused by the limited availability of resources to finance the detection drive. Since the 2000s, many authors have used this rate function or modified versions of it in their models. There have been quite a few epidemic outbursts that required widespread disease-detection drives, for instance, the recent outbreak of COVID-19. Recent studies by Al-Rifai et al. (Rami et al., 2021), Xue et al. (Xue et al., 2021) have emphasized the importance of screening in controlling the spread of COVID-19 and reducing its impact on public health. Yuan and Blakemore (Yuan & Blakemore, 2022a) have presented an observational study to emphasize the effect of testing and tracing on the COVID-19 outbreak without lockdown in Hong Kong. Nonetheless, the screening of diseases faces a potential challenge due to immigration and emigration. However, this challenge can be addressed through the application of patch modeling, as demonstrated in a recent study on COVID-19 by Das et al. (Das et al., 2023). Patch modeling is also employed in a meta-population environment, where populations are dispersed across numerous interconnected dense patches. This approach aids in comprehending the local dynamics within these patches. The COVID-19 pandemic has had a significant impact on Hong Kong, with the city facing several waves of infections since the outbreak began. The city has implemented strict social distancing measures and widespread testing to curb the spread of the virus, yet the situation remains challenging (Yuan & Blakemore, 2022b). One of the critical challenges in managing the spread of the virus in Hong Kong is balancing the need for additional screening and treatment measures to reduce transmission with the costs associated with these interventions. This observation serves as motivation for our study, in which we propose a model that addresses both the "lower petals" of the WJ screening criterion depicted in Fig. 1. We develop a model that incorporates additional screening based on infectious density and perform an analysis to determine its cost-effectiveness. Simultaneously, we examine other control intervention strategies for comparative purposes.

A study by Aleta et al. (Aleta et al., 2020) presents a mathematical model to analyze the potential effectiveness of testing, contact tracing, and household quarantine in reducing the spread of COVID-19 during the second wave of the pandemic in Boston city. One of the recent studies by Gao et al. (Gao et al., 2023) presents an *SI2A2L2R* compartmental model (considering two compartments – those with testing and those without – for each: symptomatic infectious, asymptomatic infectious, and isolated classes) to analyze how testing and isolation compliance impact early-stage COVID-19 spread, their results emphasize the importance of testing and isolation underscoring the need for other control measures. High testing rates and isolation compliance were found to notably reduce infection prevalence, particularly during daily peaks. In another study, Meijere et al. (de Meijere et al., 2023) examined the willingness of over 4594 participants across three countries to adhere to

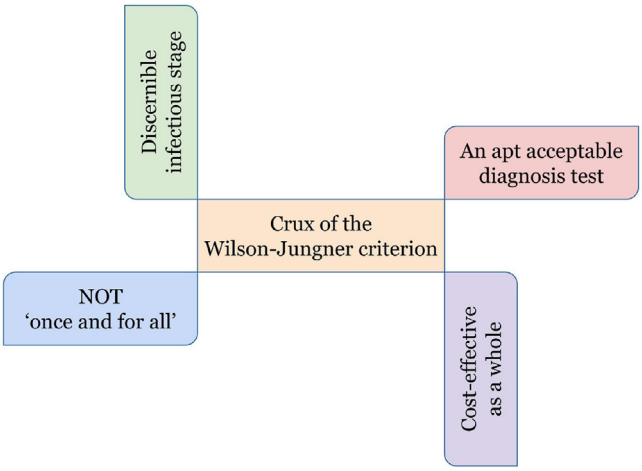

Fig. 1. Crux of WHO's Wilson-Jungner (WJ) screening criterion, developed from (Andermann et al., 2008; Maxwell Glover Wilson & Jungner, 1968). The *petal-diagram* highlights four most important crux points of WJ screening proposal. The lower two petals are most concerning as one screening strategy must not be applied once and for all, and that strategy should also be cost-effective in all aspects. Our model mainly tackles both of these issues.

testing and isolation protocols. The majority showed strong willingness for testing ($>91\%$) and rapid isolation ($>88\%$), with variations in booster vaccination adherence (73% in France, 94% in Belgium, 86% in Italy). Using modeling, they estimated substantial transmission reductions (17–24%) and decreases in the effective reproduction number (R_0) from 1.6 to 1.3 in France and Belgium, and to 1.2 in Italy, assuming declared adherence. Notably, they highlighted a potential challenge: a cost barrier to testing might compromise adherence in France and Belgium, impacting the overall effectiveness of the proposed protocols in metro cities. Indeed, to better handle the spread of the disease in a densely populated city like Hong Kong, the modelers need to incorporate and balance the additional screening and treatment measures; we propose a new approach to modeling such a situation by including additional screening based on infectious density and saturated treatment with relapse and reinfection. This type of model can help to identify high-risk areas and predict how the disease may spread in the future. We also establish an optimal control problem for the proposed model by inducting three time-dependent controls. To assess the efficiency of inducted controls, we consider various strategies with different combinations of implemented controls and perform an analysis for the cost-effectiveness of those strategies.

Cost-effectiveness analysis (CEA) is a method used to evaluate the relative efficiency of different interventions or strategies for controlling the disease. The primary aim of CEA is to identify the intervention or strategy that provides the most health benefit at the lowest cost. CEA is often used to inform decision-making in allocating resources for public health programs and policies. The 'gold-standard' book "Cost-effectiveness in health and medicine" by Weinstein et al. (Gold et al., 1996) provides an overview of the principles and methods of CEA, including the use of cost-effectiveness ratios and incremental cost-effectiveness ratios (ICERs). Recently, performing CEA for optimal control strategies has become more popular due to its ability to evaluate and compare the efficacy and efficiency of control interventions, making it particularly useful in third-world countries to manage their healthcare systems effectively. We also conduct the CEA to compare the cost-effectiveness of various strategies and determine the control intervention strategy that offers the highest cost-effectiveness in mitigating the disease burden.

The paper is primarily structured into five sections: Introduction, Material and methods, Theory and calculations, Results and discussion, and Conclusions. After giving an introduction and providing an extensive background to the research context in this section, Section 2 on 'Material and methods' presents the foundational materials and methodologies. This includes a detailed formulation of the mathematical model, as outlined in Sub-section 2.1, introducing a new concept named as infectious density-induced additional screening (IDIAS) and treatment saturation. The explanation of these two primary rate functions is presented in two separate sub-sections, leading to the subsequent derivation of the model rate equations. The Sub-section 2.1 is complemented by the validation of the model through parameter estimation and characterization using real data. Additionally, Sub-section 2.2 provides a brief summary of the methods utilized in the remaining sections of the paper. Section 3 is primarily focused on theory and calculations, which consist of two subsections: Sub-section 3.1, where we conduct an analysis of the model and reproductive threshold, including the biological feasibility of the model (3.1.1), the computation of the basic reproduction number (3.1.2), and the existence and stability of disease-free and endemic equilibria (3.1.3); while in Sub-section 3.2, we establish the optimal control problem, including the formulation of a cost functional (3.2.1), the existence and characterization of optimal controls (3.2.2), and the optimality system and solution approach (3.2.3). In section 4, we discuss the results and present a detailed discussion on numerical simulations, including the elasticity of reproduction number and effect of screening on disease spread (Sub-section 4.1), the effect of optimal control strategies that includes a detailed analysis of implementing different combinations of controls as intervention (Sub-section 4.2), cost-

effectiveness analysis of control interventions (Sub-section 4.3), and a summary of the analysis and results obtained emphasizing their public health significance (Sub-section 4.4). Finally, in Section 5, the paper is ultimately wrapped up with conclusive remarks.

2. Material and methods

This section presents all necessary material and methods, which includes a detailed explanation of the formulated model with its validation and parameter characterization, as well as a synopsis of the methods being used in the subsequent sections.

2.1. Mathematical model with IDIAS and treatment saturation

We formulate a *SI2HR* model (*I*2 denotes two infectious classes) by partitioning the total population N into five compartments, viz. susceptible S, asymptomatic infectious I_a, symptomatic infectious I_s, infective individuals under care H, and recovered R. For ease of understanding and simplicity, we have chosen not to include an exposed class of individuals in our model, as it will not significantly alter the dynamics of the disease. The population flow (see Fig. 2), in terms of the movement of individuals within a population over time through different compartments under consideration, is as follows.

$S(t)$: Susceptible individuals being recruited at the rate Λ, getting infected with the transmission rates β_s (symptomatic) and β_a (asymptomatic).
$I_a(t)$: Asymptomatic infectious individuals (mild to no symptoms), moving to H with saturated screening rate function $\varphi(I_s)$ and quarantine rate of γ. Moving to I_s with the rate of α_a.
$I_s(t)$: Symptomatic infectious individuals (mild to severe symptoms), moving to H with saturated treatment rate function $\psi(I_s)$ and quarantine rate of α_s.
$H(t)$: Infective individuals under care (isolation, quarantine, treatment, hospitalization), moving to R with a recovery rate of σ.
$R(t)$: Recovered individuals, being reinfected at a reduced rate of r by coming in contact with the infective and are moving to I_s. They are also moving back to S due to waning immunity with a rate η.

Incorporating immunity loss and reinfection in this population flow is crucial given the type of disease we are dealing with. Now, before writing the rate flow equations in mathematical form, we first elaborate the two main rate functions: $\varphi(I_s)$ – the screening rate function with infectious density-induced additional screening (IDIAS) and $\psi_1(I_s)$ – the saturated treatment rate function.

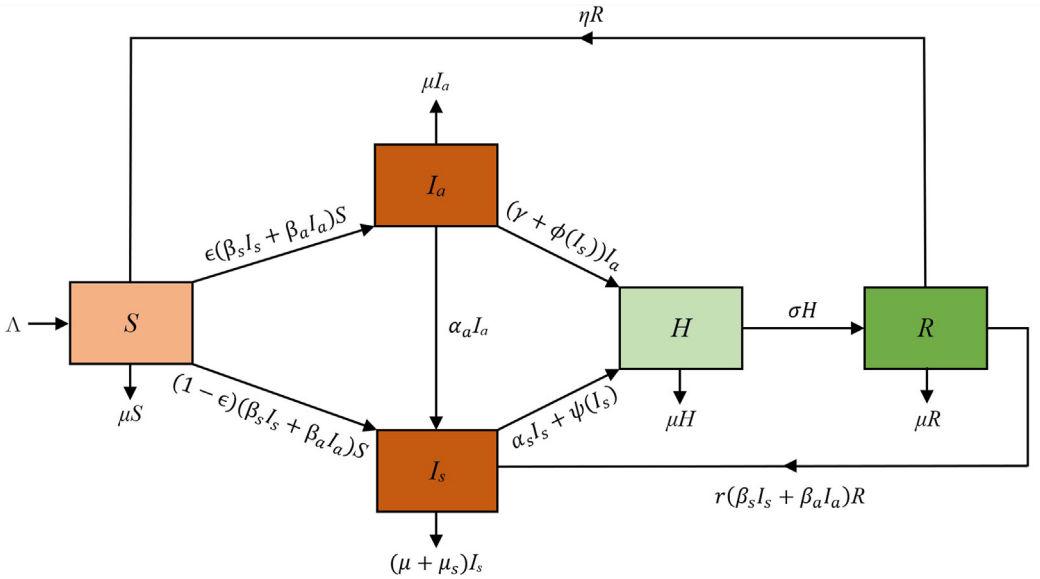

Fig. 2. Compartmental diagram depicting population flow and dynamics of the model.

2.1.1. Screening rate function with IDIAS

An additional screening prompted by the infectious density (we name it as IDIAS - infectious density-induced additional screening) along with the baseline constant screening is considered in the screening rate function,

$$\varphi(I_s) = \theta + \varphi_1(I_s) = \theta + \frac{\rho I_s}{1 + mI_s},$$

where, θ is constant baseline screening and $\varphi_1(I_s) = \frac{\rho I_s}{1+mI_s}$ is the IDIAS, where ρ is screening rate and m is saturation constant. Considering this type of screening rate function is crucial, particularly, in cases where the infectious population varies at its density. To better deal the situation in cities with dense population, an additional screening dependent on the density of infectious population along with the baseline constant screening is really important.

2.1.2. Saturated treatment rate function

The saturated treatment rate function is a commonly-used form of the treatment rate function that represents the maximum achievable treatment rate, beyond which additional treatment efforts are no longer effective in reducing the spread of the disease. The use of a saturated treatment rate function reflects the reality that there are limits to the number of individuals who can be treated in a given time frame, due to resource constraints or other practical considerations. Therefore, we incorporate the following saturated treatment rate function,

$$\psi(I_s) = \frac{\alpha I_s}{1 + \nu I_s},$$

where, α is treatment rate and ν is treatment saturation constant.

2.1.3. Compartmental flow diagram and rate equations

The mathematical model with IDIAS and treatment saturation is given by,

$$\begin{aligned}
\frac{dS}{dt} &= \Lambda + \eta R - (\beta_s I_s + \beta_a I_a)S - \mu S,\\
\frac{dI_a}{dt} &= \epsilon(\beta_s I_s + \beta_a I_a)S - (\gamma + \varphi(I_s))I_a - \alpha_a I_a - \mu I_a,\\
\frac{dI_s}{dt} &= (1-\epsilon)(\beta_s I_s + \beta_a I_a)S + \alpha_a I_a - (\alpha_s I_s + \psi(I_s)) + r(\beta_s I_s + \beta_a I_a)R - (\mu_s + \mu)I_s,\\
\frac{dH}{dt} &= (\alpha_s I_s + \psi(I_s)) + (\gamma + \varphi(I_s))I_a - \sigma H - \mu H,\\
\frac{dR}{dt} &= \sigma H - r(\beta_s I_s + \beta_a I_a)R - \eta R - \mu R,
\end{aligned} \tag{1}$$

with an initial condition setting as $(S(0), I_a(0), I_s(0), H(0), R(0))^T$ in positive $\mathbb{R}^5$. All the parameters with their values and biological meaning are given in Table 1, given in the subsection below.

Table 1
Assumed and estimated parameters and their description, unit and values/range; we obtain $\mathcal{R}_0 = 2.129$ for these parameters (P stands for 'person' and D stands for 'day' in the unit column). The estimated parameters are as per the real data from Hong Kong during the Nov–Dec 2022 time-frame.

Parameters	Description	Unit	Values/Range
Λ	Recruitment rate	$P\,D^{-1}$	Varied
ν	Treatment saturation constant	P^{-1}	0.2–0.25 (Zhang et al., 2021)
μ	Natural death rate	D^{-1}	$\frac{1}{365\times 60}$ (Assumed)
r, η	Immunity loss rate	D^{-1}	$\frac{1}{30\times 3}$ (Cristiane et al., 2021)
β_a	Disease transmission rate by asymptomatic	$P^{-1}D^{-1}$	0.00002 (Assumed)
β_s	Disease transmission rate by symptomatic	$P^{-1}D^{-1}$	0.0000001 (Estimated)
ϵ	Proportion constant for transmission ($S \to I_a$)	–	0.15–0.7 (Srivastav et al., 2021)
γ	Asymptomatic quarantine/self-isolation rate	D^{-1}	0.2–0.4 (Lin et al., 2020; Srivastav et al., 2021)
θ	Baseline screening rate	D^{-1}	0.001 (Assumed)
ρ	Additional screening rate	$P^{-1}D^{-1}$	0.005 (Estimated)
m	Screening saturation constant	P^{-1}	0.0001 (Assumed)
α_a	Conversion rate ($I_a \to I_s$)	D^{-1}	0.01–0.08 (Aldila et al., 2020)
α_s	Symptomatic quarantine/self-isolation rate	D^{-1}	0.07 (Assumed)
α	Symptomatic hospitalized rate	D^{-1}	0.02–0.1 (Li et al., 2020; Srivastav et al., 2021)
σ	Recovery rate	D^{-1}	$\frac{1}{14}$ (Lamba et al., 2023; Srivastav et al., 2021)

In infectious disease models, it is common to track the number of newly detected or infectious cases over time. However, sometimes it is useful to consider an additional rate equation to separate cumulative newly detected/infectious cases from the infectious cases that are still actively spreading the disease. Therefore, we also separate out cumulative newly detected/infected cases (denoted by$C(t)$) by the following rate equation,

$$\frac{dC}{dt} = (\alpha_s I_s + \psi(I_s)) + (\gamma + \varphi(I_s))I_a, \tag{2}$$

where, $\varphi(I_s)$ is the IDIAS rate function and $\psi(I_s)$ the treatment rate function. The need for considering an additional rate equation for $C(t)$ arises when the infectious disease model needs to capture the fact that some individuals who are infected may not be immediately detected or treated and may continue to spread the disease to others. This is especially true in the case of diseases with long incubation periods or asymptomatic carriers. By separating out the cumulative newly detected/infectious cases into a distinct rate equation, the infectious disease model can better account for the dynamics of disease transmission and the effectiveness of detection and treatment measures. This can lead to more accurate predictions of the disease spread and help in studying the impact of control measures in a better way.

2.1.4. Model validation with parameter estimation and characterization

In this subsection, we validate our model using data fitting and parameter estimation. We consider the COVID-19 cases in Hong Kong as a case study (URL) and perform data fitting in order to estimate the model parameters. We use the least square technique of data fitting. The data fitting is based on the cumulative new infective cases in Hong Kong from November 1, 2022, to December 29, 2022 (URL). Fig. 3a—a bar plot, depicts the data day-wise. So, the rate equation of $C(t)$ (*i.e.*, equation (2)) is fitted with the real data (see Fig. 3b).

2.1.4.1. Characterization of model parameters. Here, we discuss the rationale behind the values and biological essence of the literature-sourced and estimated parameters being utilized in our model formulation.

The recruitment rate Λ for susceptibles is varied around the value taken in (Saha et al., 2023), as population in the susceptible compartment can be recruited by birth, by immigration or by other means, so it can't be fixed to one value. The natural death rate μ is assumed, while the immunity loss rates r and η, representing the propensity of the recovered population to re-contract the disease and become susceptible again, respectively, are adopted from (Cristiane et al., 2021). The authors in (Cristiane et al., 2021) assume the immunity loss rate in a model formulated for Sao Paulo (one of the most populous cities in Brazil), which resembles our case of Hong Kong. The assumption is made that immunity is not permanent, and a reinfection rate of r or $\eta = 0.01$ is adopted, meaning that a recovered individual becomes susceptible again or is reinfected every 90 days by coming into contact with asymptomatic or symptomatic individuals.

The disease transmission rate by symptomatic individuals β_s and the rate of additional screening ρ are estimated using the data fitting, and to ensure the reliability of the estimates, we assumed and set the remaining parameters based on the available literature, as shown in Table 1. Since the transmission rate by the asymptomatic population is not readily accessible, we have assumed it to be higher than the transmission rate by symptomatic individuals, taking into account their higher contact rate. The proportionality constant, denoted as ϵ, signifies that ϵ fraction $(\beta_s I_s + \beta_a I_a)S$ susceptible individuals transition

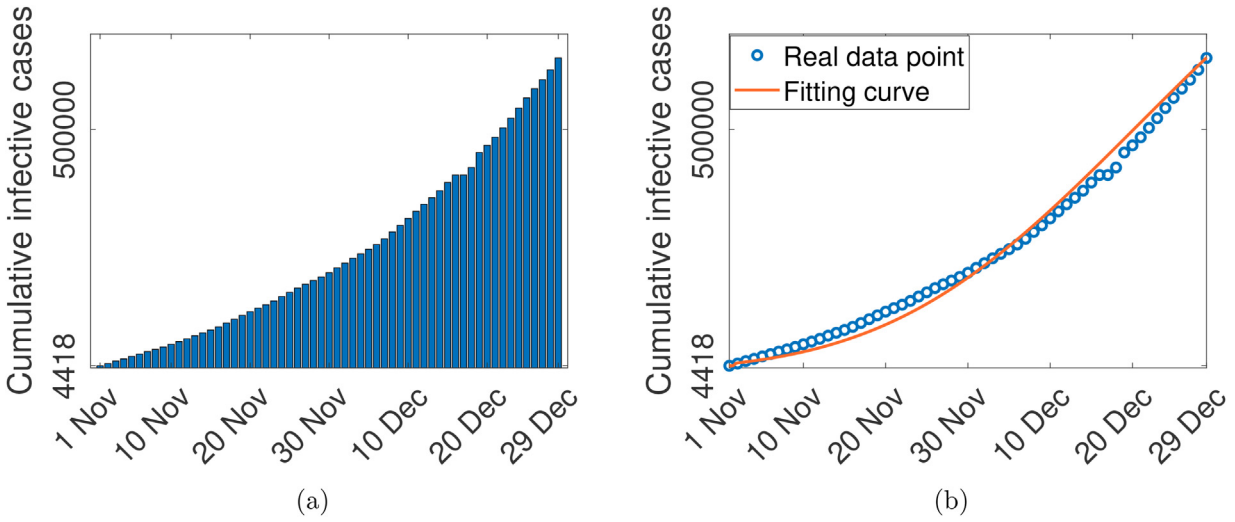

Fig. 3. (a) Depicting day-wise cumulative infective cases as per the real data of Hong Kong taken from November 1, 2022 to December 29, 2022 (b) The solution to the rate equation for $C(t)$ (representing cumulative newly detected/infectious cases), *i.e.*, solution to equation (2) is fitted with the real data.

to the I_a class, while the remaining portion, $(1-\epsilon)$ fraction, moves to the I_s class. Asymptomatic quarantine/self-isolation rate γ is sourced from (Lin et al., 2020; Srivastav et al., 2021), on the other hand, symptomatic quarantine/self-isolation rate α_s is assumed to be higher than γ. The baseline screening rate θ is assumed to be lesser than that of previous COVID waves, as our data is from the end of 2022. The screening saturation constant m and treatment saturation constant ν represents the maximum effectiveness or limit of the additional screening and treatment process as the number of symptomatic individuals (I_s) becomes very large, respectively. As I_s becomes very large, the additional screening and treatment effectiveness approaches their maximum levels $\frac{\rho}{m}$ and $\frac{\alpha}{\nu}$, determined by the screening saturation constant m and treatment saturation constant ν, respectively. This implies that even with a substantial increase in the number of symptomatic individuals being screened traditionally or treated, these processes may reach a saturation point where additional screening and treatment efforts have limited impact on the overall effectiveness. α_a represents the rate at which asymptomatic infectious individuals transition to the I_s class upon experiencing symptoms. On the other hand, α denotes the hospitalization rate for symptomatic individuals and contributes to the formulation of the saturated treatment rate function $\psi(I_s)$. The recovery rate, denoted as σ and sourced from (Lamba et al., 2023; Srivastav et al., 2021), reflects the rate at which individuals in the H class either achieve full recovery or acquire temporary or complete immunity.

2.2. Synopsis on methodologies

As mentioned in the model formulation, we have used a deterministic compartmental modeling approach, which is an evolution of the pioneer Kermack–McKendrick SIR model. For the purpose of data fitting, we employ the least square technique. We calculate the basic reproduction number using the next-generation matrix method and determine its elasticity through normalized forward sensitivity indices. The existence and stability of disease-free and endemic equilibrium points are being established using standard methods. We apply Pontryagin's maximum principle to deduce the characterization of the optimal control, and the forward-backward sweep method is employed to solve the corresponding optimality system, with detailed information provided in Sub-section 3.2.3. The cost-effectiveness analysis of various intervention strategies is primarily conducted using incremental cost-effectiveness ratios. References for all these methods are appropriately cited at their respective locations of use in the manuscript.

3. Theory and calculation

This section focuses on theory and calculations related to model analysis and the optimal control problem. In the first subsection below we majorly establish theory related to the model, including its biological feasibility, calculation of the reproduction number, and stability of the equilibria. While the Sub-section 3.2 presents the formulation of the optimal control problem with its objective cost functional and theory/calculation pertaining to the existence and characterization of the optimal controls.

3.1. Model analysis and reproductive threshold

This subsection deals with a basic analysis of the model, including a discussion on biological feasibility, *i.e.*, positivity and boundedness of the solutions; we deduce a positively invariant set that guarantees non-negativity of the solutions. We also compute the basic reproduction number using the next generation matrix (NGM) approach.

3.1.1. Biological feasibility of the model

Here, the main focus is to demonstrate the positive invariability and boundedness of the proposed model system. By showing that the model remains within biologically meaningful ranges, we can ensure that it is a viable tool for studying the behavior of the biological system of interest. This analysis is essential for assessing the model's ability to accurately reflect the real-world phenomena it aims to represent. Following (SrivastavaSonu et al., 2022; Sun et al., 2011), we state and prove the positive invariability and boundedness of the model system as.

Theorem 3.1. *The model system* (1) *is positively invariant in* $\mathbb{R}^5$ *and bounded in the region*

$$\mathcal{D} = \left\{(S, I_a, I_s, H, R) \in \mathbb{R}^5 : S \geq 0, I_a \geq 0, I_s \geq 0, H \geq 0, R \geq 0, S + I_a + I_s + H + R \leq \frac{\Lambda}{\mu}\right\}.$$

proof. *The proof is given in Appendix A.*1.

3.1.2. The basic reproduction number

System (1) has one infection-free equilibrium (IFE), denoted and given by $E_1 = (S_0,0,0,0,0) = \left(\frac{\Lambda}{\mu},0,0,0,0\right)$. Using the next generation matrix approach (Van den Driessche & James, 2002), the basic reproduction number is obtained by (details are provided in Appendix A.2),

$$\begin{aligned}\mathcal{R}_0 &= \frac{\epsilon(\alpha_s+\alpha+\mu_s+\mu)\beta_a S_0+(1-\epsilon)(\gamma+\theta+\alpha_a+\mu)\beta_s S_0+\epsilon\alpha_a\beta_s S_0}{(\gamma+\theta+\alpha_a+\mu)(\alpha_s+\alpha+\mu_s+\mu)},\\ &= \epsilon\left\{\frac{\beta_a S_0}{(\gamma+\theta+\alpha_a+\mu)}+\frac{\alpha_a}{(\gamma+\theta+\alpha_a+\mu)}\frac{\beta_s S_0}{(\alpha_s+\alpha+\mu_s+\mu)}\right\}+(1-\epsilon)\frac{\beta_s S_0}{(\alpha_s+\alpha+\mu_s+\mu)},\end{aligned} \tag{3}$$

where, $\frac{\beta_a S_0}{(\gamma+\theta+\alpha_a+\mu)}+\frac{\alpha_a}{(\gamma+\theta+\alpha_a+\mu)}\frac{\beta_s S_0}{(\alpha_s+\alpha+\mu+\mu_s)}$ represents the infection caused by an individual which was initially asymptomatic and $\frac{\beta_s S_0}{(\alpha_s+\alpha+\mu+\mu_s)}$ represents the infection caused by an individual during its symptomatic infectious period. So, the number of new infectious cases generated by a single infectious individual over the course of its life is denoted by $\mathcal{R}_0$.

Theorem 3.2. *IFE E_1 is locally stable for $\mathcal{R}_0<1$ and unstable for $\mathcal{R}_0>1$.*
proof. The proof is given in Appendix A.3.

Theorem 3.3. At $\mathcal{R}_0 = 1$, the backward bifurcation occurs for $\nu > \nu_{crit}$ and forward (transcritical) bifurcation occurs for $\nu < \nu_{crit}$, where ν_{crit} is defined in the proof.
proof. *The proof is given in Appendix A.*4.

It is important to highlight that a larger value for ν indicates the presence of a backward bifurcation, resulting in the persistence of the disease. This underscores the crucial role played by the treatment saturation constant ν in the eradication of the disease when $\mathcal{R}_0<1$. This correlation makes sense, as a higher ν is associated with a lengthier waiting time for treatment, thereby amplifying the chances of infection spread and contributing to the sustained presence of the disease.

3.1.3. Existence and stability of endemic equilibria

System (1) has endemic equilibrium $E_2^* = (S^*, I_a^*, I_s^*, H^*, R^*)$ where,

$$H^* = \frac{\alpha_s I_s^* + \psi(I_s^*) + (\gamma+\varphi(I_s^*))I_a^*}{\sigma+\mu}, \quad R^* = \frac{\sigma H^*}{r(\beta_s I_s^*+\beta_a I_a^*)+\eta+\mu}, \quad S^* = \frac{\Lambda+\eta R^*}{\beta_s I_s^*+\beta_a I_a^*+\mu}. \tag{4}$$

We express R^* and S^* of (4) in terms of I_a^* and I_s^* as follows,

$$R^* = \frac{\sigma(\alpha_s I_s^* + \psi(I_s^*) + (\gamma+\varphi(I_s^*))I_a^*)}{(\sigma+\mu)(r(\beta_s I_s^*+\beta_a I_a^*)+\eta+\mu)} := g_1(I_a^*, I_s^*), \tag{5a}$$

$$S^* = \frac{\mu S_0}{\beta_s I_s^*+\beta_a I_a^*+\mu} + \frac{\eta g_2(I_a^*, I_s^*)}{\beta_s I_s^*+\beta_a I_a^*+\mu} := g_2(I_a^*, I_s^*). \tag{5b}$$

Substitute H^*, R^* and S^* from (5) in differential equations $\frac{dI_a}{dt}\Big|_{E_2^*} = 0$ and $\frac{dI_s}{dt}\Big|_{E_2^*} = 0$ we have,

$$\begin{aligned} g_3(I_a^*, I_s^*) &:= \epsilon(\beta_s I_s^*+\beta_a I_a^*)g_3(I_a^*, I_s^*) - (\gamma+\varphi(I_s^*)+\alpha_a+\mu)I_a^* = 0,\\ g_4(I_a^*, I_s^*) &:= (1-\epsilon)(\beta_s I_s^*+\beta_a I_a^*)g_3(I_a^*, I_s^*) + \alpha_a I_a^* - (\alpha_s I_s^* + \psi(I_s^*)) + r(\beta_s I_s^*+\beta_a I_a^*)g_2(I_a^*, I_s^*) - (\mu_s+\mu)I_s^* = 0.\end{aligned}$$

So, all $S^*, I_a^*, I_s^*, H^*, R^*$ are positive if $g_3(I_a^*, I_s^*) = 0$ and $g_4(I_a^*, I_s^*) = 0$ give positive real root. Therefore, either unique endemic equilibrium or multiple endemic equilibria may exist, respectively, if $g_3(I_a^*, I_s^*) = 0$ and $g_4(I_a^*, I_s^*) = 0$ have one positive root or many positive roots. Although we cannot prove the existence of endemic equilibrium for $\mathcal{R}_0>1$, the numerical result for specific parameter values (given in Sub-section 2.1.4) indicates the existence of an endemic equilibrium for $\mathcal{R}_0>1$.

Theorem 3.4. *The endemic equilibrium E_2^* is locally stable if* $b_0>0$, $b_4>0$, $b_4b_3-b_2>0$, $b_2(b_4b_3-b_2)-b_4(b_4b_1-b_0)>0$, *and* $(b_2(b_4b_3-b_2)-b_4(b_4b_1-b_0))(b_4b_1-b_0)-b_0(b_4b_3-b_2)^2>0$, *where* b_0, b_1, b_2, b_3, *and* $b_4$are given *in* (14).
proof. The proof is given in Appendix A.5.

3.2. Establishment of optimal control problem

In this subsection, we formulate an optimal control problem for the model system (1) by introducing three time-varying controls. After inducting the control variables $u_1(t)$, $u_2(t)$, and $u_3(t)$, we get the following corresponding dynamical system with controls,

$$\begin{aligned}
\frac{dS}{dt} &= \Lambda + \eta R - (1-u_1(t))(\beta_s I_s + \beta_a I_a)S - \mu S,\\
\frac{dI_a}{dt} &= \epsilon(1-u_1(t))(\beta_s I_s + \beta_a I_a)S - \left(\gamma + \theta + \frac{\rho u_2(t) I_s}{1+mI_s}\right) I_a - \alpha_a I_a - \mu I_a,\\
\frac{dI_s}{dt} &= (1-\epsilon)(1-u_1(t))(\beta_s I_s + \beta_a I_a)S + \alpha_a I_a - \left(\alpha_s I_s + \frac{\alpha u_3(t) I_s}{1+\nu I_s}\right) + r(\beta_s I_s + \beta_a I_a)R - (\mu+\mu_s) I_s,\\
\frac{dH}{dt} &= \left(\alpha_s I_s + \frac{\alpha u_3(t) I_s}{1+\nu I_s}\right) + \left(\gamma + \theta + \frac{\rho u_2(t) I_s}{1+mI_s}\right) I_a - \sigma H - \mu H,\\
\frac{dR}{dt} &= \sigma H - r(\beta_s I_s + \beta_a I_a)R - \eta R - \mu R,
\end{aligned} \tag{6}$$

with initial populations $(S(0), I_a(0), I_s(0), H(0), R(0))^T \in \mathbb{R}^5_+$. Given the financial constraints on the healthcare system, intervention policies must also be limited (Gaff & Schaefer, 2009; Kumar et al., 2017a, 2017b). Therefore, we take all three controls as bounded in [0, 1], where attaining the upper bound represents the maximum efforts required.

1. **Precautionary measures** $u_1(t)$ applied to susceptibles, which includes disease prevention efforts by sanitation, masking, and social distancing. The term $(1-u_1(t))$ signifies the ultimate reduction in the transmission rate as an increase in $u_1(t)$ implies a decrease in $(1-u_1(t))$.
2. **Boosted screening** $u_2(t)$ for asymptomatic infectives. The multiplication of $u_2(t)$ with the additional screening (IDIAS) rate function $\varphi_1(I_s)$ represents a boost in the infectious density-induced additional screening for the infectives. The assignment $u_2(t) = 1$ denotes screening efforts at full potential, while $u_2(t) = 0$ represents only a baseline constant screening is being carried out, *i.e.*, no additional screening.
3. **Boosted treatment** $u_3(t)$ for symptomatic infectives. The multiplication of $u_3(t)$ with the treatment rate function $\psi(I_s)$ denotes treatment boost. The value $u_3(t) = 0$ quantify that treatment is not available.

3.2.1. Designing objective cost functional

Before establishing the existence and characterization of optimal controls, we first design the cost functional with various cost components that are to be optimized (minimization of disease prevalence and cost incurred). The following is the objective cost functional corresponding to system (6),

$$\mathcal{J}(u_1(t), u_2(t), u_3(t)) = \int_0^{t_f} \left[C_1 I_a(t) + C_2 I_s(t) + C_3 H(t) + \frac{1}{2}\left(C_4 u_1^2(t) + C_5 u_2^2(t) + C_6 u_3^2(t)\right)\right] dt. \tag{7}$$

$\mathcal{J}(u_1(t), u_2(t), u_3(t))$ represents the total cost incurred due to intervention policies, which is a weighted sum of different components: the cost due to prevalence,

$$\int_0^{t_f} (C_1 I_a(t) + C_2 I_s(t) + C_3 H(t)) dt,$$

we consider this as directly proportionate to the number of individuals who are infectious (including asymptomatic and symptomatic individuals as well as those under medical care), which reflects the social and economic impact of the disease prevalence. The cost incurred due to precautionary measures,

$$\int_0^{t_f} C_4 u_1^2(t) dt,$$

the cost of boosting screening,

$$\int_0^{t_f} C_5 u_2^2(t)dt,$$

and cost of boosting treatment,

$$\int_0^{t_f} C_6 u_3^2(t)dt.$$

The second-order non-linearity in these cost components pertains to a non-linear increase in cost incurred due to implementing these controls to cover a large population. Now on, we will use u_1, u_2, and u_3 instead of $u_1(t)$, $u_2(t)$, and $u_3(t)$ for simplicity and denotation.

Our primary objective is to reduce disease prevalence while minimizing the cost. In other words, we aim to identify an optimal set of controls (u_1^*, u_2^*, u_3^*) that achieves this objective,

$$\mathcal{J}(u_1^*, u_2^*, u_3^*) = \min\{\mathcal{J}(u_1, u_2, u_3) : u_1, u_2, u_3 \in A_U\},$$

where, $A_U = \{(u_1, u_2, u_3)$: u_1, u_2, u_3 are measurable, $0 \le u_1, u_2, u_3 \le 1$, $t \in [0, t_f]\}$ is the set of admissible controls. The positive coefficients in the integrand of (7), C_1, C_2, C_3, C_4, C_5, and C_6 are the constants that not only balance the weighted cost-sum but also signify the importance of a particular component.

3.2.2. Optimal controls: existence and characterization

Here, we present the necessary and sufficient conditions for solving the optimal control problem. Prior to outlining the characterization, we examine the sufficient condition for optimal controls, as outlined in Theorem 2.1. in (Lenhart & Workman, 2007), Theorem 4.1 in (Wendell et al., 2012), Theorem 9 in (SrivastavaSonu et al., 2022), and related corollaries. We utilize Pontryagin's maximum principle (PMP) (Lenhart & Workman, 2007) to deduce the characterization of the optimal controls, *i.e.*, necessary conditions. Since u_i (for $i = 1, 2, 3$) are bounded, therefore, the state variables s_i (for $i = 1, 2, 3, 4, 5$) of the model system (6) are also bounded in $\mathcal{D}$, as discussed in Sub-section (3.1). We represent the vector $\mathbf{s} = [s_i]$ as the vector of state variables $s_1 = S$, $s_2 = I_a$, $s_3 = I_s$, $s_4 = H$, $s_5 = R$ and the vector $\mathbf{u} = [u_i]$ as the vector of control variables $u_1, u_2, u_3 \in A_U$.

Theorem 3.5. (*Sufficient Condition*) *Consider* $\mathcal{R}(t, \mathbf{s}, \mathbf{u})$ *be the right hand side of the equations in system* (6) *and* $\mathcal{I}(t, \mathbf{s}, \mathbf{u}) = C_1 I_a(t) + C_2 I_s(t) + C_3 H(t) + \frac{1}{2}\left(C_4 u_1^2(t) + C_5 u_2^2(t) + C_6 u_3^2(t)\right)$ *be the term under integral sign in the objective functional* (7) *then a optimal triplet of controls* (u_1^*, u_2^*, u_3^*) *exists if following criteria are met*:

1. $\mathcal{R}$ *is of class* C^1 *and there exist positive constants* P_1, P_2, P_3 *such that* $|\mathcal{R}(t,0,0)| \le P_1$, $|\mathcal{R}_{\mathbf{s}}(t,\mathbf{s},\mathbf{u})| \le P_2(1 + |\mathbf{u}|)$, $|\mathcal{R}_{\mathbf{u}}(t,\mathbf{s},\mathbf{u})| \le P_3$,
2. The feasible solution set $\mathcal{D}$swith controls in A_U is non-empty and bounded,
3. $\mathcal{R}(t, \mathbf{s}, \mathbf{u}) = \mathcal{F}(t, \mathbf{s}) + \mathcal{G}(t, \mathbf{s})\mathbf{u}$,
4. *The set* $A_U = [0, 1] \times [0, 1]$ *is bounded, closed, and convex,*
5. $\mathcal{I}$is convex *in* A_U.

Proof. Proof is done as per the approach followed in (SrivastavaSonu et al., 2022) and is omitted here.

Now, in order to make use of the PMP, we formulate the Hamiltonian $\mathcal{H}(\mathbf{s}, \mathbf{u}, \lambda)$, which is a sum of the integrand $\mathcal{I}(t, \mathbf{s}, \mathbf{u})$ and $\sum_{i=1}^{5} \lambda_i \frac{ds_i}{dt}$, given by,

$$\mathcal{H}(\mathbf{s}, \mathbf{u}, \lambda) = \mathcal{I}(t, \mathbf{s}, \mathbf{u}) + \lambda_1 \frac{dS(t)}{dt} + \lambda_2 \frac{dI_a(t)}{dt} + \lambda_3 \frac{dI_s(t)}{dt} + \lambda_4 \frac{dH(t)}{dt} + \lambda_5 \frac{dR(t)}{dt},$$

where, $\lambda = (\lambda_1, \lambda_2, \lambda_3, \lambda_4, \lambda_5) \in \mathbb{R}^6$ is known as adjoint vector, elements of which satisfies,

$$\frac{d\lambda_1(t)}{dt} = -\frac{\partial \mathcal{H}}{\partial S}, \frac{d\lambda_2(t)}{dt} = -\frac{\partial \mathcal{H}}{\partial I_a}, \frac{d\lambda_3(t)}{dt} = -\frac{\partial \mathcal{H}}{\partial I_s}, \frac{d\lambda_4(t)}{dt} = -\frac{\partial \mathcal{H}}{\partial H}, \text{ and } \frac{d\lambda_5(t)}{dt} = -\frac{\partial \mathcal{H}}{\partial R}, \tag{8}$$

with transversality conditions $\lambda_1(t_f) = 0$, $\lambda_2(t_f) = 0$, $\lambda_3(t_f) = 0$, $\lambda_4(t_f) = 0$, and $\lambda_5(t_f) = 0$.

Theorem 3.6. *(Necessary Condition) Given the existence of an optimal control triplet* (u_1^*, u_2^*, u_3^*) *and the corresponding quintet (S*, I_a^*, I_h^*, H, R*) that optimize the objective cost functional* (7)*, there exist* λ_1, λ_2, λ_3, λ_4, *and* λ_5, *satisfying the adjoint system* (8) *with transversality conditions, then the triplet of optimal controls can be characterized as* (u_1^*, u_2^*, u_3^*), *where,*

$$
\begin{aligned}
u_1^* &= \max\left\{\min\left\{\frac{(\epsilon\lambda_2-(1-\epsilon)\lambda_3-\lambda_1)(\beta_s I_s^*+\beta_a I_a^*)S^*}{C_1},1\right\},0\right\},\\
u_2^* &= \max\left\{\min\left\{\frac{(\lambda_2-\lambda_4)\rho I_s^* I_a^*}{C_5(1+mI_s^*)},1\right\},0\right\},\\
u_3^* &= \max\left\{\min\left\{\frac{(\lambda_3-\lambda_4)\alpha I_s^*}{C_6(1+\nu I_s^*)},1\right\},0\right\}.
\end{aligned}
\tag{9}
$$

Proof. Proof is done as per the approach followed in (SrivastavaSonu et al., 2022) *and is omitted here.*

3.2.3. Optimality system and solution approach

The optimality system for our model consists of the state equation (6) with initial conditions, the adjoint system (8) with transversality conditions, and the optimality conditions (9). This optimality system, as a whole, is termed as the optimal control problem. The solution approach for optimal control problems typically involves formulating a mathematical model that describes the behavior of the system being controlled, defining an objective function that specifies the desired behavior or performance of the system, and then using optimization algorithms to find the control inputs that optimize the objective function subject to any constraints on the system. There are various techniques and algorithms for solving optimal control problems, including direct methods (such as the shooting method and the collocation method) and indirect methods (such as the Pontryagin's maximum principle and the Hamilton-Jacobi-Bellman equation). The choice of method depends on the specific characteristics of the problem, such as the dimensionality of the system, the nature of the objective function and constraints, and the desired accuracy and computational efficiency of the solution.

The forward-backward sweep method (FBSM) is a well known numerical optimization technique used for solving optimal control problems. The method involves breaking the problem into two parts: the forward sweep, which involves simulating the controlled system (6) forward in time to generate a guess for the control inputs, and the backward sweep, which involves solving the adjoint system (8) backwards in time to obtain the sensitivities of the objective functional (7) with respect to the state variables and control inputs. Using these sensitivities, the control inputs are updated in the forward sweep, and the process is iterated until convergence is achieved. To solve the adjoint system and control system backward and forward in time, respectively, we employ the fourth-order Runge-Kutta method, a widely-used numerical method for approximating the solutions to differential equations with high accuracy. The FBSM has the advantage of being relatively simple to implement and computationally efficient, particularly for problems with a large number of control variables.

4. Results and discussion

In this section, we present and discuss the results of our numerical simulations investigating the effects of various factors on the reproduction number ($\mathcal{R}_0$) and disease spread. Specifically, we explore the impact of screening and the variation of other key parameters on $\mathcal{R}_0$ and disease spread. We present the results of our numerical simulations by using line and contour plots to illustrate visually. These plots provide a clear representation of the relationship between different parameters and the key outcomes of interest. Additionally, we show the effect of using different combination of optimal controls on the disease spread. We also analyze the cost-effectiveness of various screening and control strategies, with the aim of identifying the most efficient and effective approaches for managing the disease.

4.1. Elasticity of $\mathcal{R}_0$ and effect of screening on disease spread

Variation in transmission rate, screening rate, quarantine rates, and treatment rate can have a significant impact on the reproduction number ($\mathcal{R}_0$) and the spread of a disease. Elasticity is a measure of how sensitive a variable is to changes in another variable. In this case, it refers to how sensitive $\mathcal{R}_0$ is to changes in factors like transmission rate, screening rate, quarantine rates, and treatment rate. Knowing the elasticity of $\mathcal{R}_0$ allows us to quantify the impact of changes in these factors on the spread of a disease.

4.1.1. Elasticity of $\mathcal{R}_0$

We see in expression (3) that the symptomatic disease transmission rate (β_s), screening rate (θ), quarantine rates (γ, α_s), and treatment rate (α) all have an effect on the basic reproduction number. With respect to these parameters (β_s, θ, γ, α_s, and α), the normalized forward sensitivity index (also known as elasticity) is computed to quantify the change in basic reproduction number when the corresponding parameter changed. Following the approach given by Bonyah et al. (Bonyah et al., 2017) elasticity of $\mathcal{R}_0$ with respect to parameter x is given by,

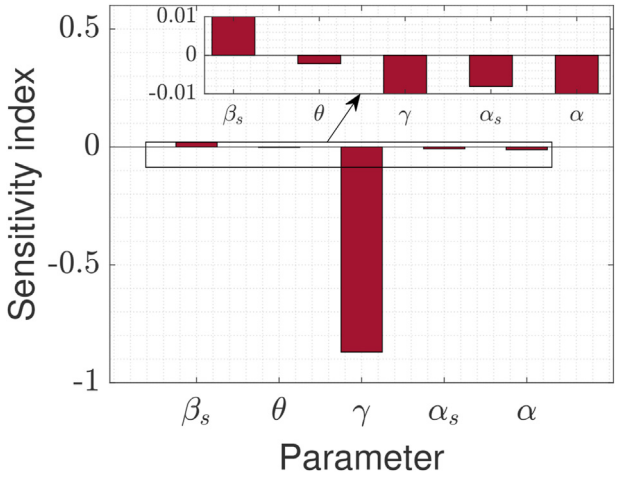

Fig. 4. Normalized sensitivity index (elasticity) of $\mathcal{R}_0$ with respect to symptomatic disease transmission rate β_s, baseline screening rate θ, quarantine/self-isolation rates γ and α_s, and treatment rate α; among these parameter, γ is the most sensitive. The negative sensitivity index of γ shows that delaying quarantine/self-isolation of asymptomatic individual will cause huge surge in the reproduction number. *i.e.*, new infections.

Table 2
Effective $\mathcal{R}_0$ range with respect to the ranges of different control measures.

Control parameter range	Effective $\mathcal{R}_0$ range for 60 days
$u_1 \in [0, 1], u_2 = 0, u_3 = 0$	$\mathcal{R}_0 \in [0.9763, 2.1739]$
$u_2 \in [0, 1], u_1 = 0, u_3 = 0$	$\mathcal{R}_0 \in [0.5381, 2.8993]$
$u_3 \in [0, 1], u_1 = 0, u_2 = 0$	$\mathcal{R}_0 \in [0.8381, 1.3138]$

$$E_x^{\mathcal{R}_0} = \frac{x}{\mathcal{R}_0} \bullet \frac{\partial \mathcal{R}_0}{\partial x}.$$

This expression measures the percentage change in $\mathcal{R}_0$ resulting from a 1% change in the parameter x, assuming all other factors remain constant. For instance, in Fig. 4, the positive sensitivity index (+0.015) of parameter β_s implies that a 1% rise in the β_s value increases the R_0 by 0.015%. So the basic reproduction number increases as the disease transmission rate by symptomatic individuals grows. The negative sensitivity index of parameters γ, α_s, and α indicates that raising the values of these parameters decreases $\mathcal{R}_0$. This leads to the conclusion that delaying in screening, quarantining, or treating any individual will raise the basic reproduction number.

4.1.2. Effective $\mathcal{R}_0$ (with respect to controls)

While the parameters appearing in the expression for $\mathcal{R}_0$ exert a significant influence on it (as seen in sensitivity analysis given above), the control variables used in the model system 6 can also wield considerable impact. Here, we observe changes in the reproductive threshold with respect to the ranges of different control measures. We used the approach given in (Lamba et al., 2023) to calculate $\mathcal{R}_0$ in terms of control variables and to obtain the effective $\mathcal{R}_0$ ranges. As an example, to determine the effective range of $\mathcal{R}_0$ with respect $0 \leq u_1 \leq 1$, we maintained other control variables at their minimum values and varied u_1 from its lower to upper bounds over the duration of control implementation, *i.e.*, 60 days, and derived a range for the effective reproduction number. Similarly, effective ranges for $\mathcal{R}_0$ are determined for the other two control variables, as indicated in Table 2 below.

Here, the upper limit of control variables signifies the maximum level of implementation efforts, while the lower limit represents their absence in the model system. We observe that employing only u_1, i.e., relying solely on precautionary measures, leads to a reduction in the $\mathcal{R}_0$ value from 2.1739 to 0.9763; only boosting additional screening, i.e., using only u_2 as a control measure, results in a decrease in the $\mathcal{R}_0$ value from 2.8993 to 0.5381; and only boosted treatment efforts, i.e., only u_3, reduces the $\mathcal{R}_0$ value from 1.3138 to 0.8381. The average of the upper bounds of effective $\mathcal{R}_0$ corresponds to the basic reproduction number (without controls), which is $\mathcal{R}_0 = 2.129$, as indicated in the caption of Table 1.

4.1.3. Effect of screening

To see the effect of screening in slowing the disease spread, we assume that a baseline screening with the rate θ and an additional screening with the screening rate ρ and saturation constant m are both available. To quantify the screening effect on the infective population, we vary the parameters θ, ρ, and m.

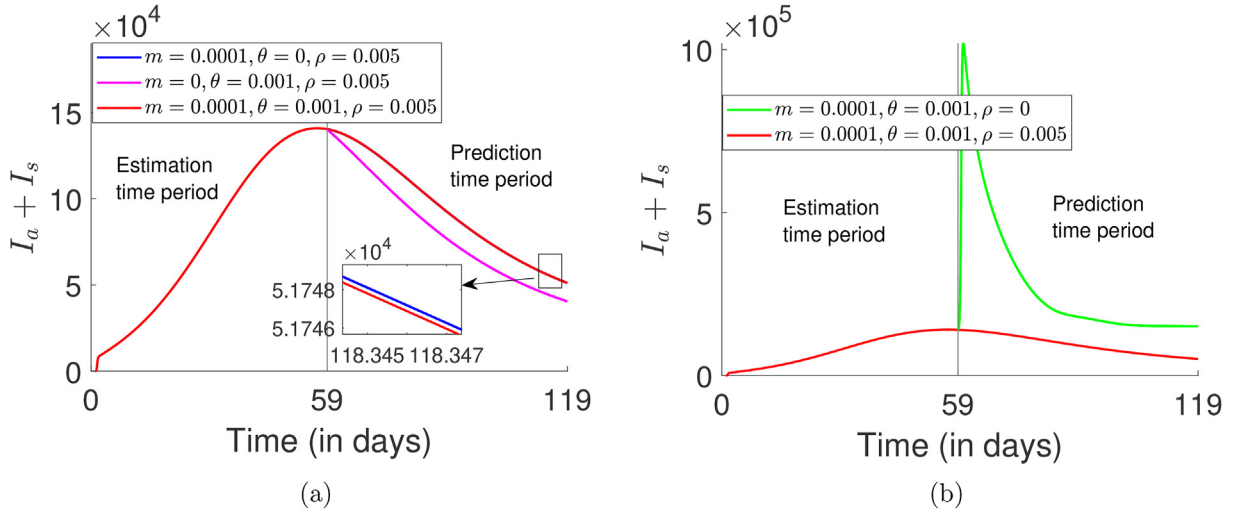

Fig. 5. Evolution in total number of infectives when screening saturation m, baseline screening θ, and additional screening ρ are varied; (a) shows that stopping baseline screening ($\theta = 0$) causes increase in infectives, while providing linear screening ($m = 0$) decreases the infectives level (b) shows that disease infection may surge without additional screening.

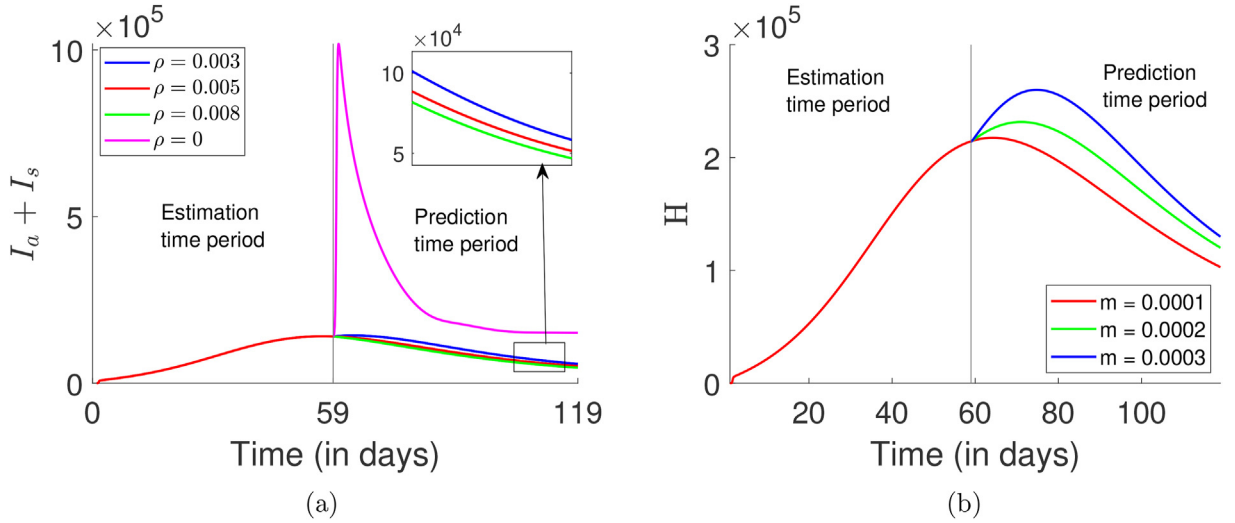

Fig. 6. (a) Evolution in total number of infectives as per variation in additional screening rate ρ; the graph shows that increasing additional screening rate ρ can reduce the infectives, while stopping it ($\rho = 0$) may cause a sudden surge in cases, (b) depicts that increasing saturation level in IDIAS term may cause an increased burden on hospitalization.

Fig. 5a depicts the evolution of total infective individuals ($I_a + I_s$) as the above mentioned parameters vary. We investigate four distinct cases of parameter variation. The red curve in Fig. 5a and b is plotted when both screenings are available. In comparison to this red curve, we obtained that stopping the additional screening (*i.e.*, $\rho = 0$) increases the infective individual level (green curve in Fig. 5b), stopping the baseline screening (*i.e.*, $\theta = 0$) increases the infective individual level (magenta curve in Fig. 5a), and providing linear additional screening (*i.e.*, $m = 0$) decreases the infective individual level (blue curve in Fig. 5a).

The curve in Fig. 5b also suggests that the disease infection is very high without additional screening. This suggests that disease control without the support of additional screening is not a viable option. Fig. 6a depicts the evolution of the total number of infective individuals ($I_a + I_s$) as screening rate ρ varied. It shows that increasing the screening rate ρ of additional screening reduces the infective individual level. While Fig. 6b shows that increasing saturation level m in the IDIAS term, *i.e*, delay in additional screening induced by infectious density may cause an increased burden by surging the number of individuals under care H.

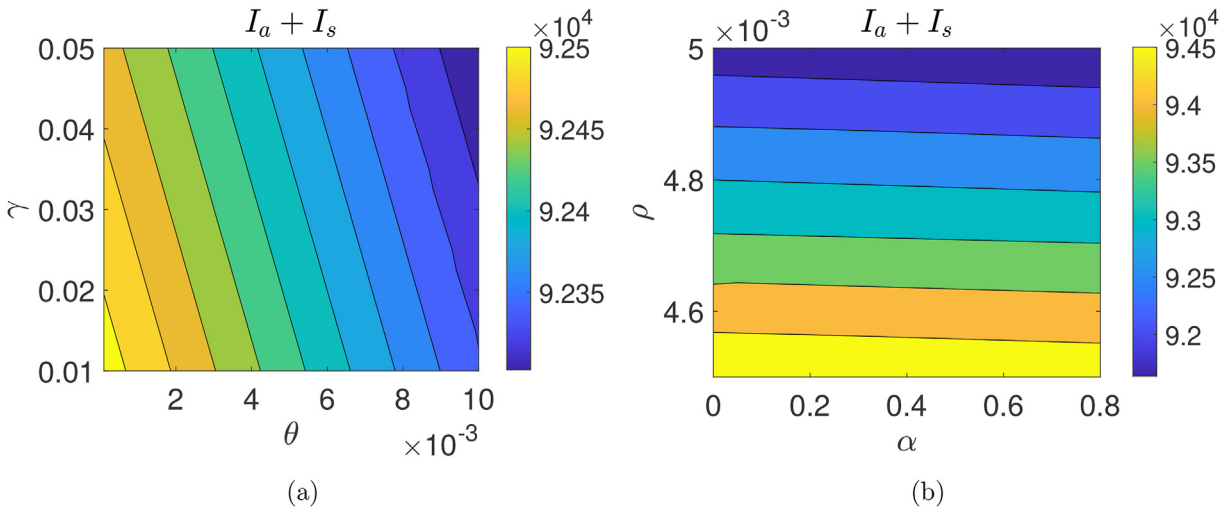

Fig. 7. Contour plots depicting evolution in number of infectives when γ, θ, ρ, and α are varied; (a) increasing in baseline screening rate θ and quarantine/self-isolation rate γ, however, increasing baseline screening rate is more impactful in comparison to the increase in quarantine/self-isolation rate (b) Shows increase in additional screening rate ρ is quite impactful in decreasing infectives but increasing in hospitalization rate α is not much helpful in reducing number of infectives.

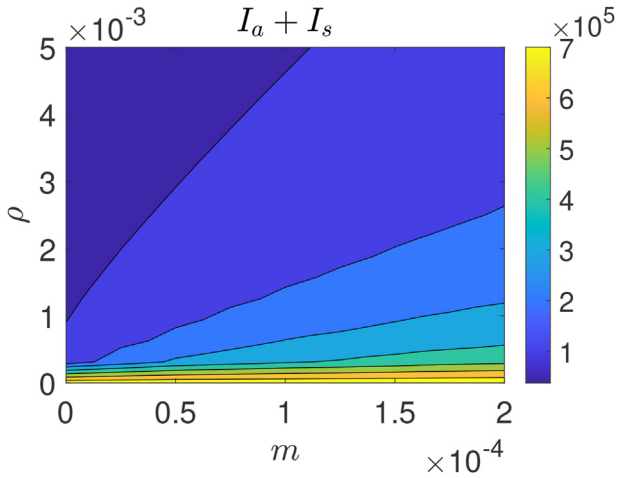

Fig. 8. Contour plot showing effect of varying additional screening rate ρ and the saturation level m on number of infectives; taking saturation level $m \in (0, 0.0002)$ and increasing the additional screening is beneficial in diseasing the number of infectives. Note that increasing the saturation level while keeping the additional screening rate to the minimum shows intangible impact, on the other hand, increasing the additional screening while keeping the saturation level below 1×10^{-4} has a huge impact on decreasing the disease burden by reducing number of infectives ($I_a + I_s$).

Fig. 7a, a contour plot with respect to θ and quarantine rate of asymptomatic individual γ, depicts the total infective individuals, $I_a + I_s$, obtained for various values of $\theta(\in (0, 0.001))$ and $\gamma(\in (0.01, 0.05))$. Fig. 7a illustrates that as θ or γ increases, the number of infective individuals decreases. Fig. 7b—a contour plot with respect to treatment rate α and screening rate in additional screening ρ, depicts the total infective individuals, $I_a + I_s$, obtained for various values of $\alpha(\in (0, 0.8))$ and $\rho(\in (0.0045, 0.005))$. Fig. 7b illustrates that as ρ or α increases, the number of infective individuals decreases.

Fig. 8 shows that increasing additional screening rate only (ρ only) is helpful in reducing the infectives (similar to Fig. 7b); however, increasing only saturation level in the IDIAS term causes increase in infectives.

Thus, it is concluded that baseline screening rate, screening rate of additional screening, saturation level of additional screening, and quarantine rate of the asymptomatic individuals have a major role in slowing the disease spread.

4.2. Effect of optimal control strategies

In order to numerically simulate the optimal control problem, we have chosen a specific set of parameters from Table 1: $\Lambda = 30$, $\beta_a = 0.00002$, $\mu = 0.0000425$, $\eta = 0.01$, $\gamma = 0.4$, $\epsilon = 0.4$, $\sigma = 1/14$, $\alpha_a = 0.04$, $\alpha_s = 0.09$, $\mu_s = 0.0052$, $\alpha = 0.1$, $\nu = 0.2$,

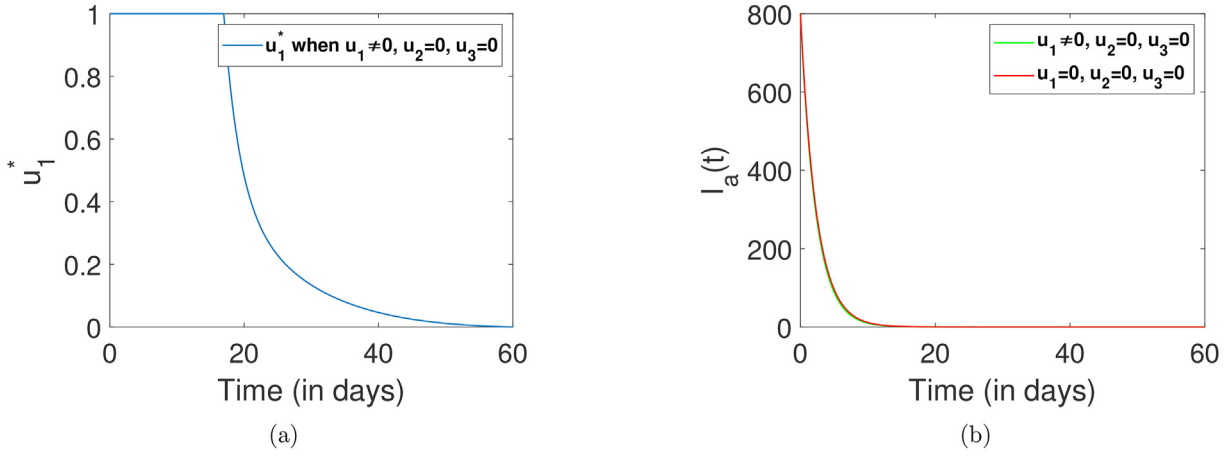

Fig. 9. (a) Optimal profile for u_1, when only u_1 is applied, *i.e.*, implementation of only precautionary measures (b) Plot for asymptomatic infectives $I_a(t)$ when only u_1 is applied as a control intervention (red curve is when no controls are applied), this suggests that there is a very little variation in the number of asymptomatic cases when only precautionary measure are applied as intervention.

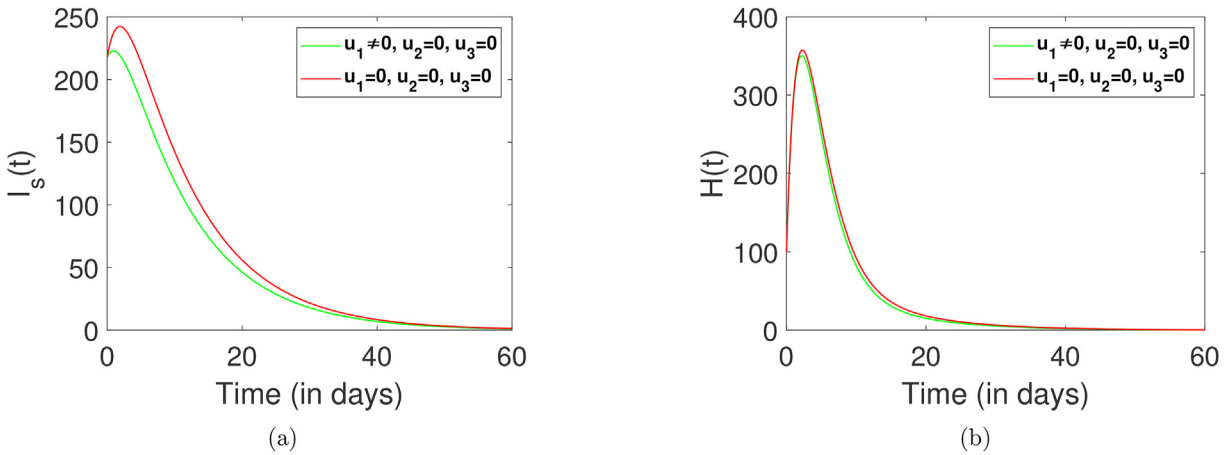

Fig. 10. (a) Plot depicting evolution symptomatic infectives $I_s(t)$ when only u_1 is applied in comparison with the evolution when no control is employed (b) Plot for evolution of hospitalized or individuals under care $H(t)$, when only u_1 is applied as a control intervention (red curves are when no control is applied). These graphs shows that implementation of only precautionary measures as an intervention is more effective in the evolution of symptomatic infectives and individuals under care than that of asymptomatic infectives.

$\theta = 0.001$, $\rho = 0.005$, $m = 0.0001$, $\beta_s = 0.0000001$, $r = 0.01$ with $(2000, 800, 218, 100, 0)$ as populations at the initial time. These values have been selected based on a careful consideration of the nature of the system and the goals of the simulation. To further optimize our simulation, we have also assigned weights to the objective functional. The weights for different components of the objective functional are $C_1 = 10$, $C_2 = 10$, $C_3 = 15$, $C_4 = 10$, $C_5 = 20$, and $C_6 = 10$. These weights reflect the varying importance of the cost-components and efforts required for each of the different control interventions. We consider the control implementation for a time period of 60 days. Below is a detailed analysis of implementing different combinations of control interventions, which helped us to draw some interesting conclusions.

4.2.1. The case when $u_1 \neq 0$ and $u_2 = 0 = u_3$, i.e., application of only u_1 as control

The implementation of only precautionary measure as a control intervention, although, keeps the green curves (with application of control) below the red curves (without any control), but is not much effective for asymptomatic infectives (I_a) and individuals under care (H) (see Figs. 9b and 10b). Fig. 9a depicts the optimal path for u_1, that physically represents efforts required for the implementation of u_1 as control. It roughly requires around 17 days of full efforts before slowly coming down. While Fig. 10a represents that applying only precautionary measures as a control is helpful in taking the number symptomatic infectives a little down, which might be reduce the disease burden up to some extent. This shows that implementation of only u_1 is very little helpful in reducing the disease burden and cost incurred (see Fig. 11).

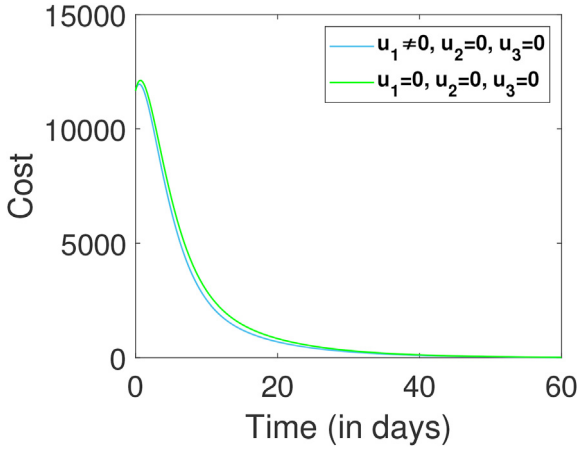

Fig. 11. Cost incurred with application of u_1 (blue curve) and without control (green cure), graph shows that even application of only precautionary measures as control can keep the cost incurred below the cost incurred when no control is applied.

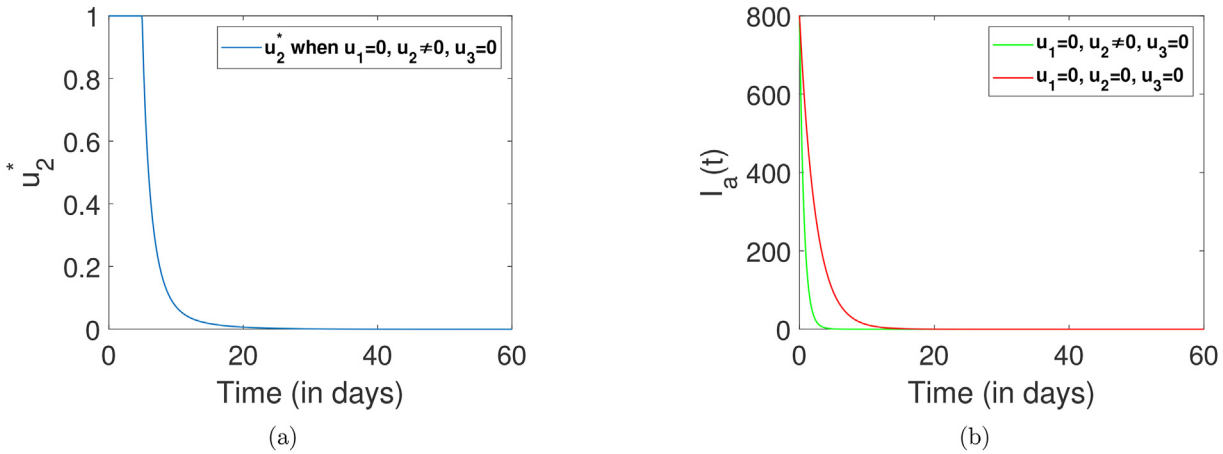

Fig. 12. (a) Optimal profile for u_2 when only u_2 is applied, *i.e.*, only boosted screening is considered as an intervention, which in comparison to the previous case when only precautionary measures are applied requires around five days of full efforts before it slowly comes down (b) Plot for evolution of asymptomatic infectives $I_a(t)$, when only u_2 is applied as a control intervention (red curve is when no control is applied). It can be observed that this strategy is quite helpful in tumbling down even the asymptomatic infectives, unlike the previous case.

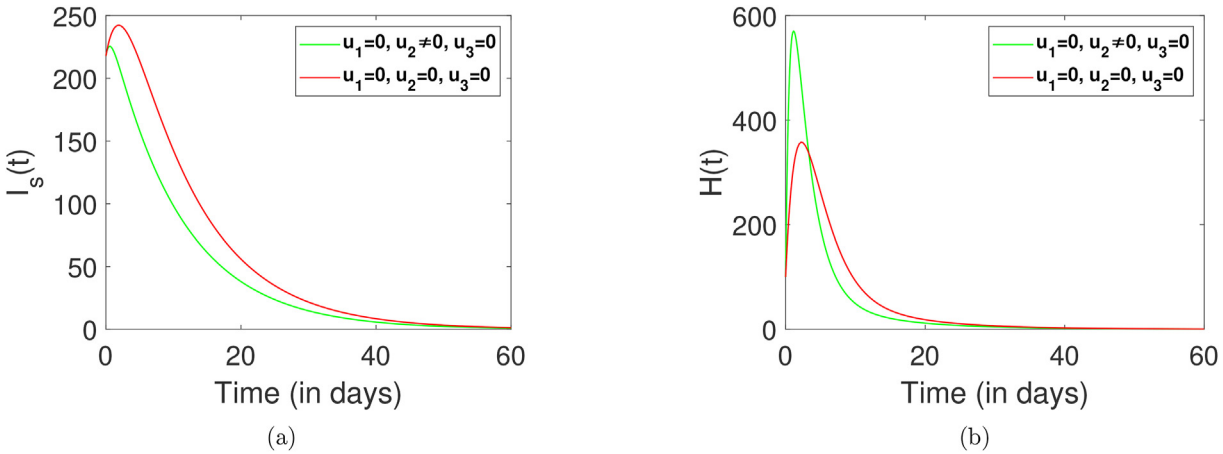

Fig. 13. (a) Plot (green curve) for symptomatic infectives $I_s(t)$ when only boosted screening is applied (b) Plot for individuals under care $H(t)$ when only u_2 is applied as a control intervention (in comparison to the red curves when no control is applied).

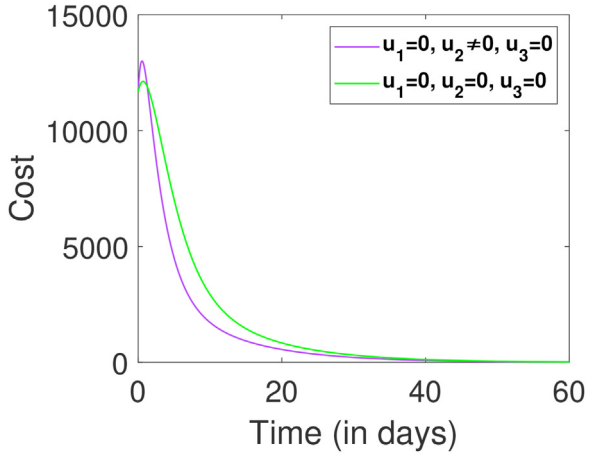

Fig. 14. Cost incurred with application of only u_2 (magenta curve) and without control (green cure). It shows that implementation of only boosted screening is quite helpful in keeping the cost incurred below the cost incurred due to disease burden when no control is applied.

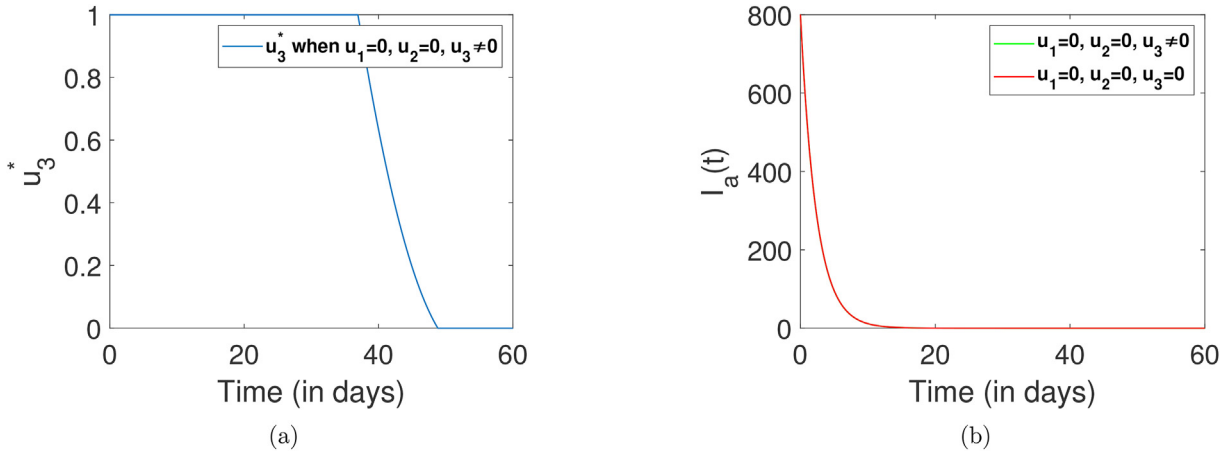

Fig. 15. (a) Optimal profile for u_3, when only boosted treatment is considered as an intervention, it requires even more number days with full efforts than that of previous two cases (b) Plot for asymptomatic infectives $I_a(t)$, when only u_3 is applied as a control intervention (red curve is when no control is applied). It is evident is that this control intervention is not much promising in reducing asymptomatic cases.

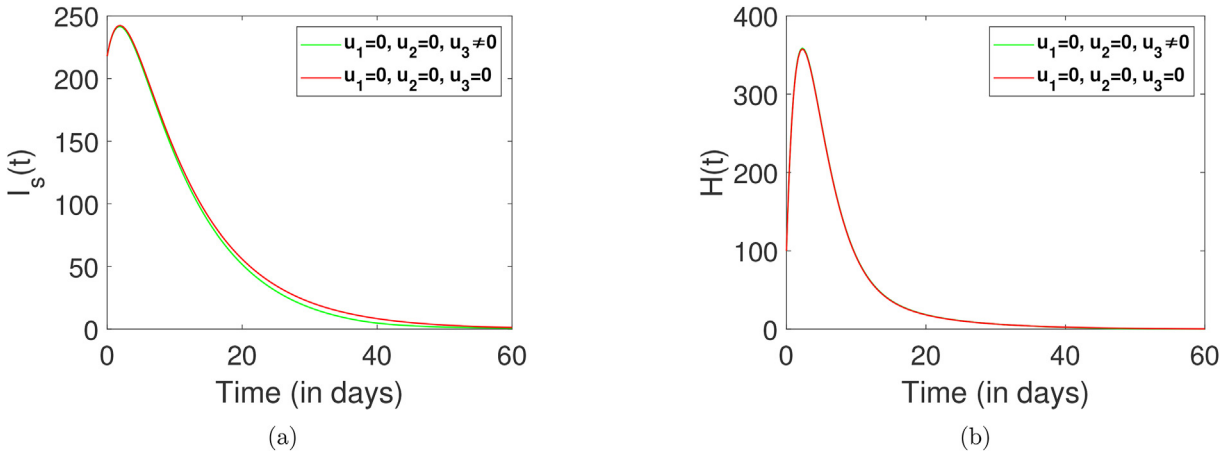

Fig. 16. (a) Plot for symptomatic infectives $I_s(t)$ (b) Plot for individuals under care $H(t)$, when only u_3 is applied as a control intervention (red curves are when no control is applied). It shows that only boosted treatment as a control strategy has minute impact on symptomatic infective and almost ineffective on individuals under care, unlike the previous two cases.

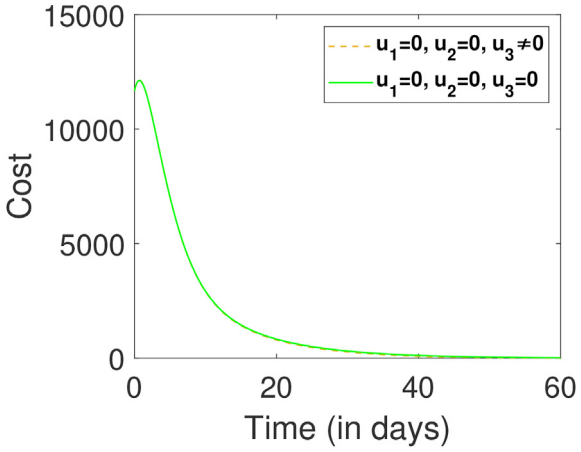

Fig. 17. Cost incurred due to application of only u_3 (dotted yellow curve) and without control (green cure). It shows that only boosting treatment cannot be a viable option as it doesn't lower down the cost incurred due to the disease burden, therefore, it might need inclusion of other intervention or control measures.

4.2.2. The case when $u_2 \neq 0$ and $u_1 = 0 = u_3$, i.e., application of only u_2 as control

The application of only boosted screening as a control intervention looks promising by looking at the simulation graphs. Fig. 12a depicts that for achieving the possible objective goal, it requires full efforts of boosted screening for just 5 initial days before the requirement slows down to zero after 20 days. Figs. 12b and 13a show that boosting screening is quite helpful in tumbling down the number of asymptomatic and symptomatic infectives.

On the other hand, Fig. 13b represents a realistic fact that on boosting screening number of individuals under care (quarantine or hospitalized) will defiantly increases initially before coming down (even below the red cure, *i.e.*, when no controls are applied) eventually. The cost profile for this case is shown in Fig. 14 above.

4.2.3. The case when $u_3 \neq 0$ and $u_1 = 0 = u_2$, i.e., application of only u_3 as control

Employing only boosted treatment as a control seems to be a redundant intervention because even after putting full efforts for 37 days (as shown in Fig. 15a) it does not have much impact on any of the infective populations, except a little decrement in the symptomatic individuals (see Fig. 16b). One more reason why we say it as a redundant strategy is that because it does not contribute in decreasing the cost incurred due to disease burden and control application (see Fig. 17). However, we will investigate benefits (if any) of this intervention in comparison with the other strategies in the cost-effectiveness analysis in the subsequent section.

4.2.4. The case when $u_1 \neq 0$, $u_2 \neq 0$, and $u_3 = 0$, i.e., application of both u_1 and u_2 as control

The application of both u_1, *i.e.*, precautionary measures and u_2, *i.e.*, boosted screening seem to be effective to reduce the disease burden to an extent. Fig. 18a and b show that simultaneous application of both controls extends the number of days required with full efforts, here precautionary measures are needed to be employed for a longer period than that of

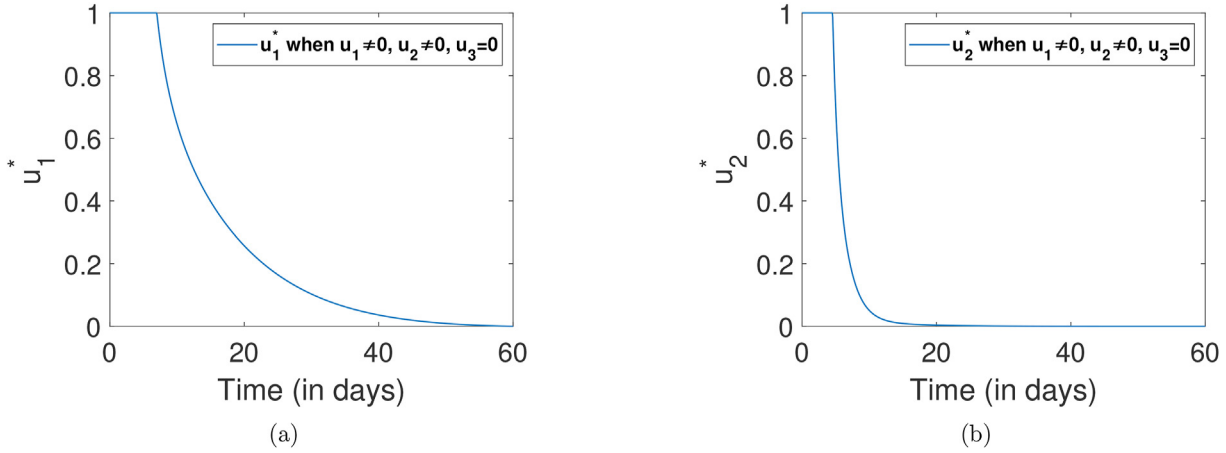

Fig. 18. Optimal path (a) for u_1 (b) for u_2, when both u_1 and u_2, *i.e.*, simultaneous application of both precautionary measures and boosted screening.

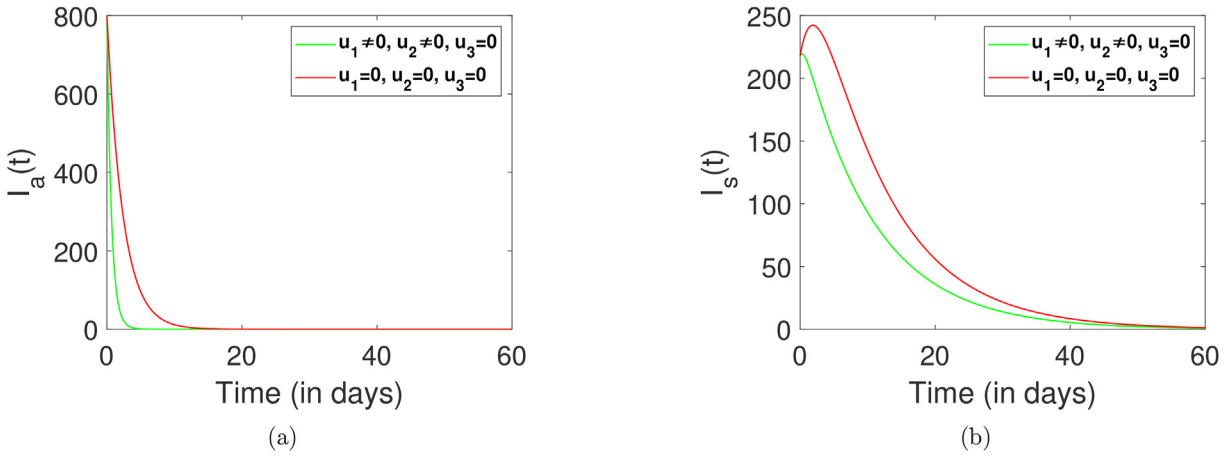

Fig. 19. (a) Plot for evolution of asymptomatic infectives $I_a(t)$ (b) Plot for symptomatic infectives $I_s(t)$, green curves are when both u_1 and u_2 are applied (red curves are when no control is applied). The graphs depicts that combining boosted screening with precautionary measures have even better impact on disease prevalence in comparison with the case where application of only precautionary measures is considered as a control intervention.

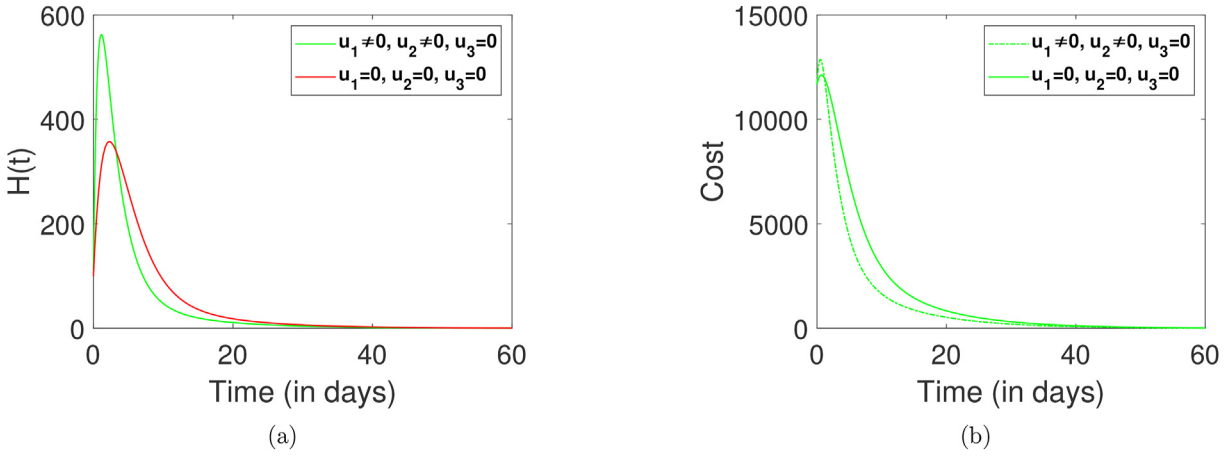

Fig. 20. (a) Plot for evolution of individuals under care $H(t)$, when both u_1 and u_2 are applied as a control intervention (red curve is when no control is applied) (b) Cost incurred with (dotted green curve) and without control (green cure).

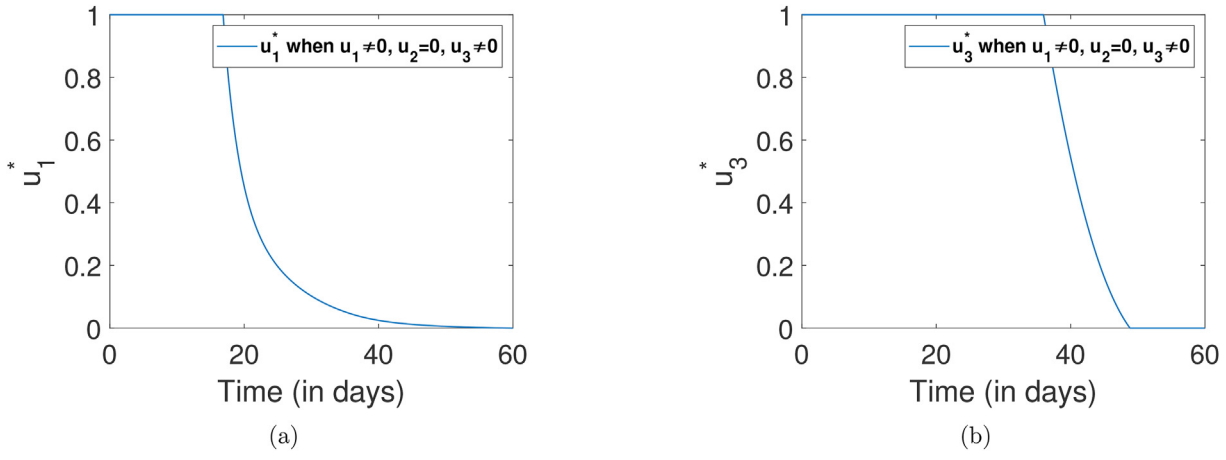

Fig. 21. Optimal control paths for (a) u_1 and (b) u_3, when both u_1 and u_3 are applied, *i.e.*, combined implementation of boosted treatment and precautionary measures.

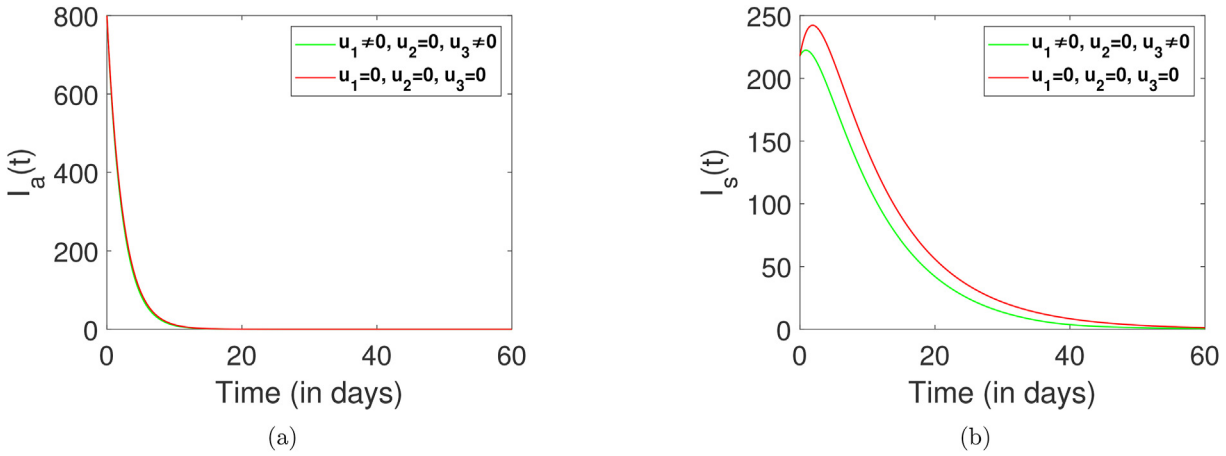

Fig. 22. Disease prevalence curves (a) For asymptomatic infectives I_a and (b) For symptomatic infectives I_s, green curves are when both u_1 and u_3 are applied (red curves are when no control is applied). These graph shows that inclusion of precautionary measures to the strategy when only boosted treatment was considered as a control makes it more impactful for symptomatic infectious individuals.

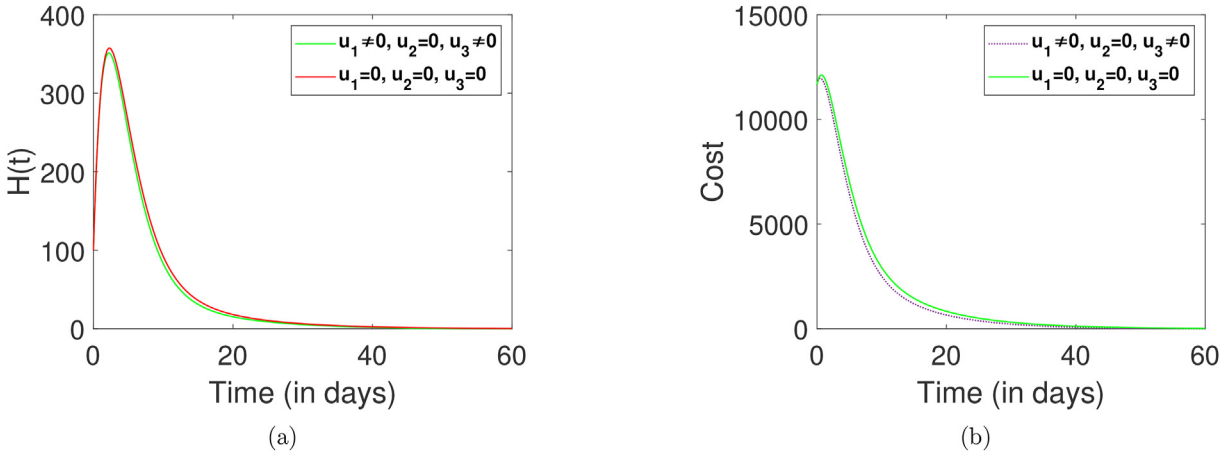

Fig. 23. (a) Disease prevalence curve for individuals under care H and (b) Cost profile, when both u_1 and u_3 are applied in comparison with the case when no controls are applied. It shows that there is a positive impact on individuals under care and cost profile when precautionary measures are considered in addition to the boosted treatment.

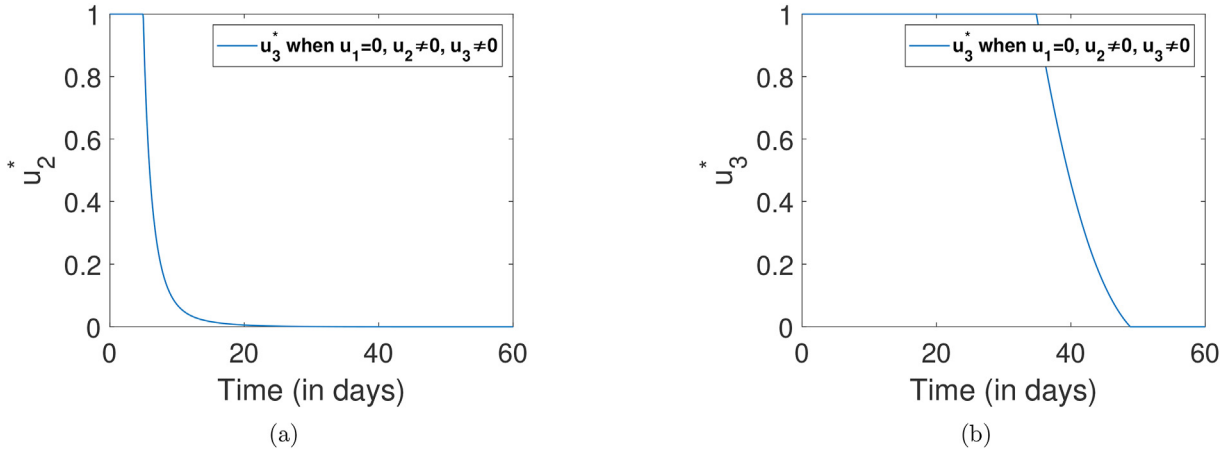

Fig. 24. Optimal control paths for (a) u_2 and (b) u_3, when both u_2 and u_3 are applied, *i.e.*, combined implementation of boosted screening and boosted treatment.

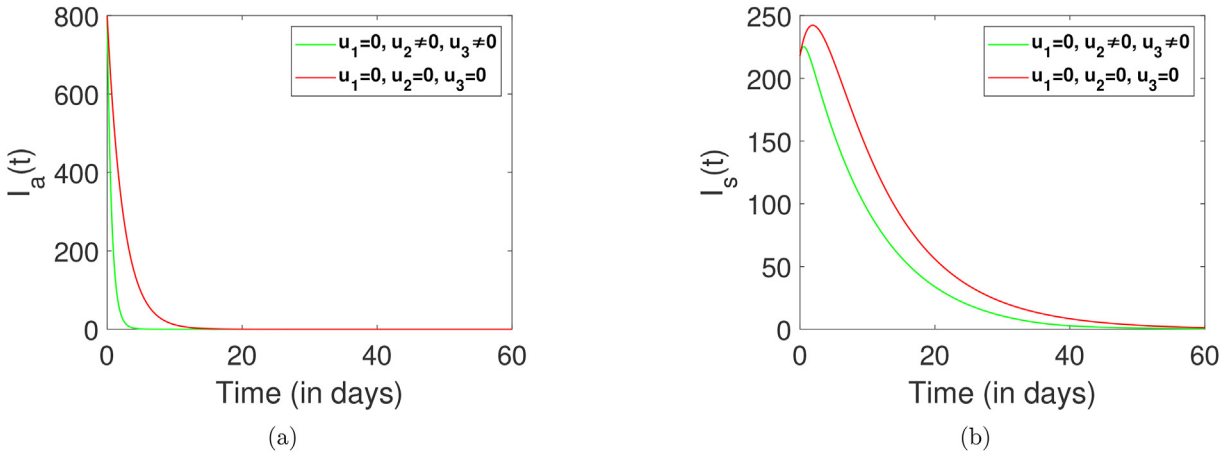

Fig. 25. Disease prevalence curves (a) for asymptomatic infectives I_a and (b) For symptomatic infectives I_s, green curves are when both u_2 and u_3 are applied (red curves are when no control is applied).

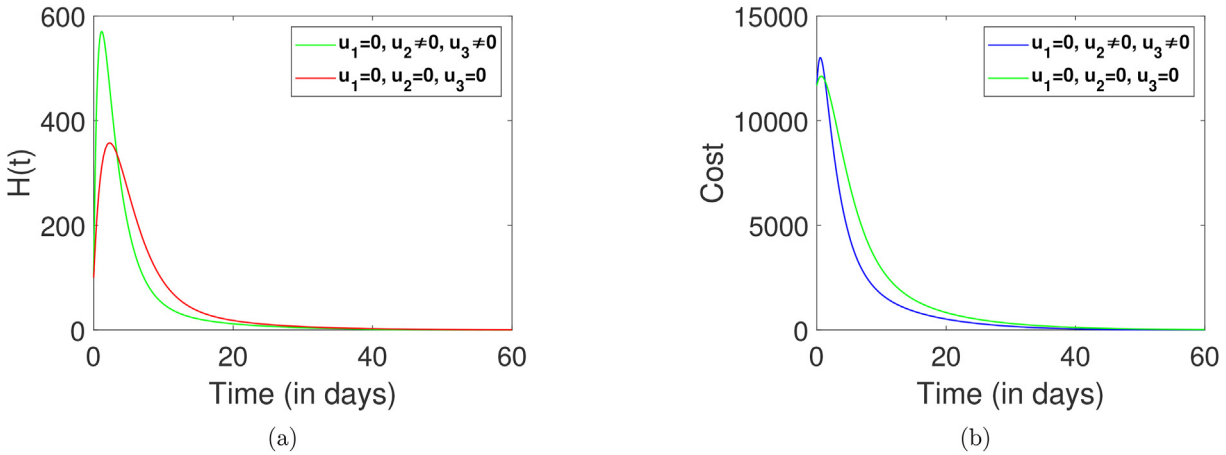

Fig. 26. (a) Disease prevalence curve for individuals under care H, when both u_2 and u_3 are applied (green), red curve is when no control is applied and (b) Cost profiles with (blue) and without controls (green). The cost profile shows that boosting both the screening and treatment have even better impact on reducing the cost incurred due to disease prevalence and the cost of control implementation.

employment of only u_1 as control (see Fig. 9a). This because of the availability of same resources, therefore, to achieve the optimality with application of two controls at time, efforts need to be increased. Fig. 19a, b, and 20a have similar argument to the case when only u_2 is applied and show that implementation of both u_1 and u_2 is quite helpful in reducing the number of infective cases as well as the cost incurred (as shown in Fig. 20b).

4.2.5. The case when $u_1 \neq 0$, $u_3 \neq 0$, and $u_2 = 0$, i.e., application of both u_1 and u_3 as control

The graphs show that the combination of implementing precautionary measure and boosted treatment has some positive impact on number of symptomatic infectives (as shown in Fig. 22b), in comparison with the separate implementation of u_1 and u_3, see Figs. 10a and 16a, respectively (see Fig. 23a for impact of this strategy on infectives under care H(t) and see Fig. 23b for cost profile). The optimal control paths for this case are shown in Fig. 21.

4.2.6. The case when $u_2 \neq 0$, $u_3 \neq 0$, and $u_1 = 0$, i.e., application of both u_2 and u_3 as control

When both u_2 and u_3 are applied, it can be seen (in Fig. 24a) that the full efforts of boosted treatment (u_3) are required for longer period as compared to the boosted screening u_2 (see Fig. 24b). This strategy seems to be promising in reducing both asymptomatic and symptomatic infectives (see Fig. 25a and b). Also, the hospitalized populations goes to a peak initially but then eventually comes below the curve (red) without control (see Fig. 26a), while keeping the cost mostly below the cost of disease burden when no control is applied (see Fig. 26b).

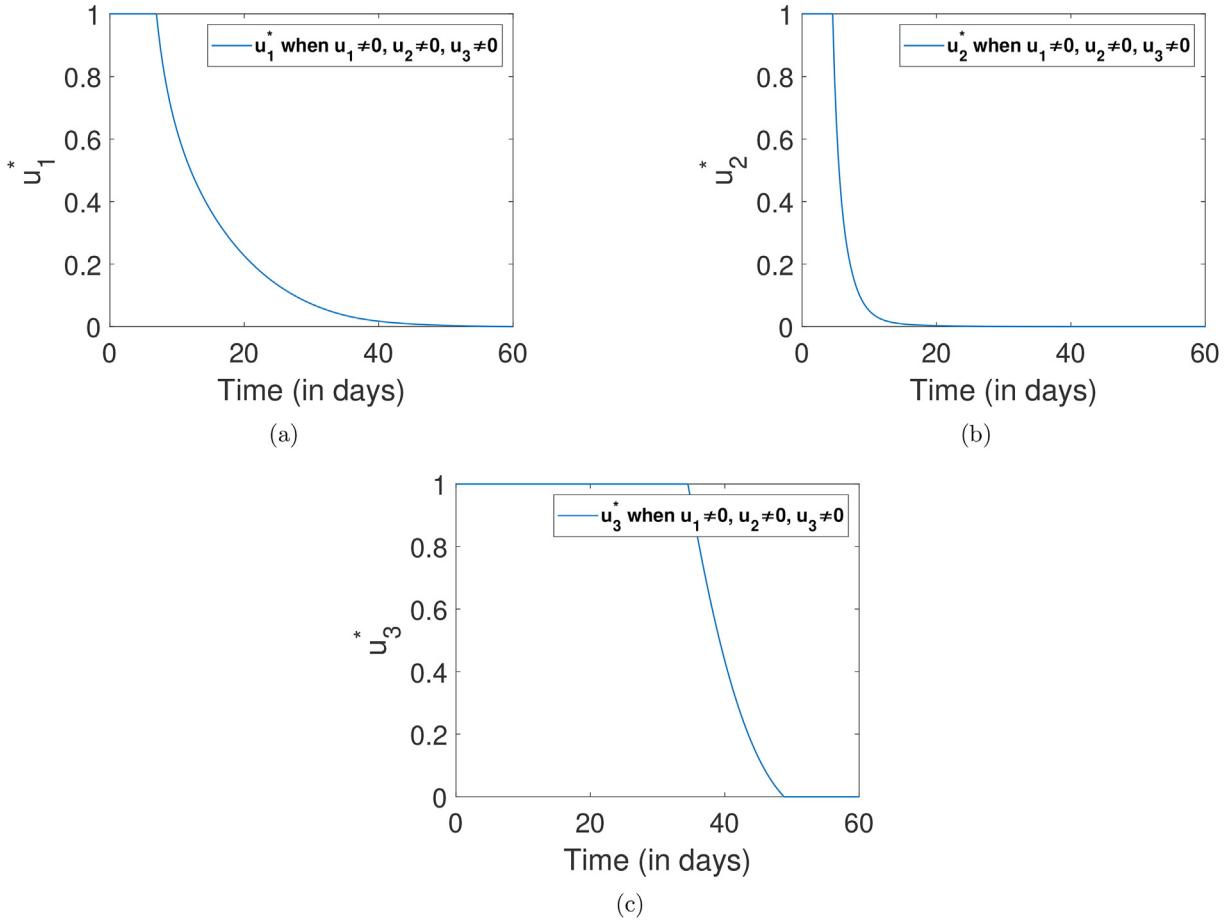

Fig. 27. Optimal control paths for (a) u_1, (b) u_2, and (c) u_3, when all controls are applied at the same time.

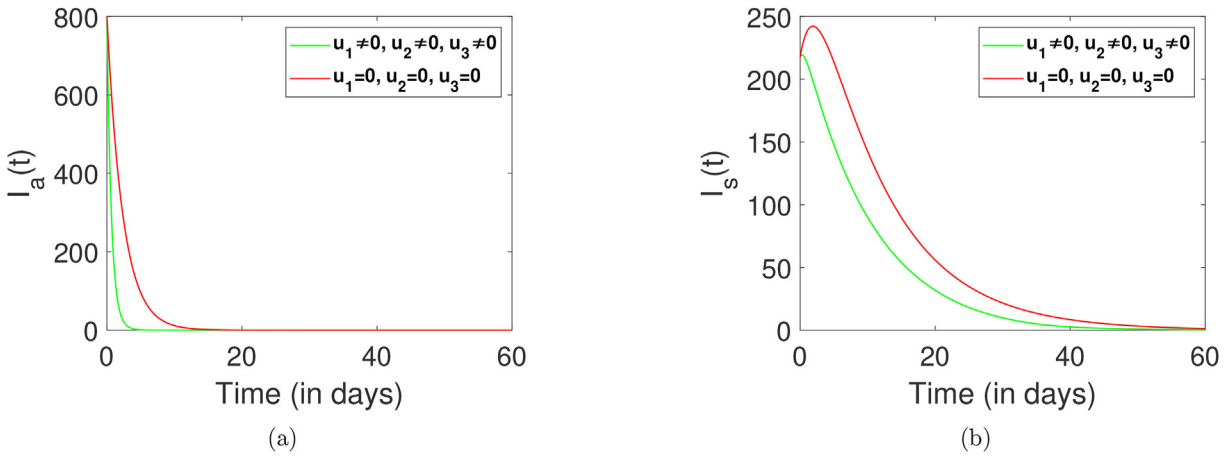

Fig. 28. Disease prevalence curves (a) for asymptomatic infectives I_a (b) For symptomatic infectives I_s, with all three controls (green) and without application of controls (red).

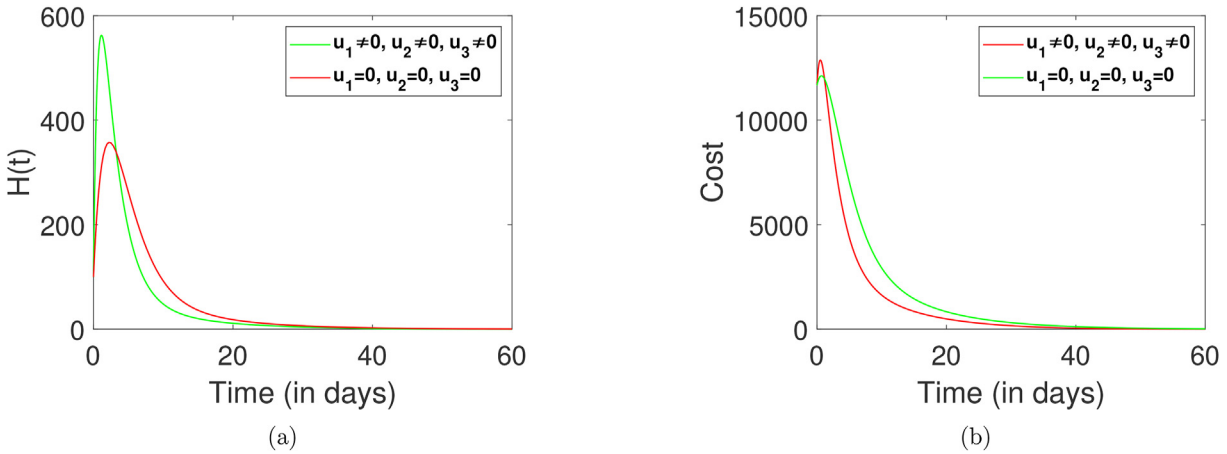

Fig. 29. (a) Disease prevalence curves for individuals under care H, when all controls are applied simultaneously (red curve is when no control is applied); and (b) Cost profile with (green) and without application of controls (red).

4.2.7. The case when $u_1 \neq 0$, $u_2 \neq 0$, $u_3 \neq 0$, i.e., simultaneous application of all controls

One interesting observation is that whenever boosting screening is included as control in any intervention strategy, for instance, in strategy when u_2 is applied with u_1 or u_3 or both (last case), there is a sudden increment in the cost profile for some initial days and then cost incurred goes down the curve when no controls are applied (as shown in Figs. 20b, 26b and 29b). But those increments come with a justification that whenever boosting screening is combined with any of the other controls as an intervention, there are positive effects on disease prevalence as well (see Fig. 28 and Fig. 29). More proper explanation is given in the next subsection. The optimal control paths for this case are shown in Fig. 27.

Through this discussion, we have gained an understanding of how various control interventions can have varying impacts on both disease prevalence and associated costs. Nevertheless, determining the most effective control intervention strategy from the range of cases analyzed can be challenging. As a result, we will conduct a cost-effectiveness analysis in the following subsection.

4.3. Cost-effectiveness analysis of control strategies

The primary aim of cost-effectiveness analysis (CEA) is to identify the intervention or strategy that provides the most health benefit at the lowest cost. CEA is often used to inform decision-making in allocating resources for public health programs and policies. There are three primary techniques (Agusto & ELmojtaba, 2017) for this analysis, which are described below.

4.3.1. Averted infections ratio

The averted infections ratio (AIR) is given by,

$$\text{AIR} = \frac{\text{Number of averted infections}}{\text{Number of recovered}}.$$

The number of staved-off (averted) infections is the total infections that would have occurred without the implementation of control measures, minus the total infections that occur after the implementation of control measures. The most effective strategy is the one with the highest averted infection rate (AIR). This approach is limited to evaluating individual strategies and does not allow for the analysis of the combination of strategies. Furthermore, this technique does not take into account the costs incurred by the implementation of control measures, therefore, other methods may be needed to address this limitation.

4.3.2. Average cost-effectiveness ratio

The average cost-effectiveness ratio (ACER) is appropriate for the cost analysis of one intervention strategy at a time. The ACER is given by,

$$\text{ACER} = \frac{\text{Total cost incurred due to strategy implementation}}{\text{Total number of cases averted by using that strategy}}.$$

Eradication and control of any disease(s) can be very expensive; therefore, determining the most cost-effective strategy or combination of strategies is necessary. The lower value of the ACER implies better cost-efficiency of that particular strategy, but to compare two or more strategies we need study the incremental cost-efficacy. For that purpose, we need the incremental cost-effectiveness ratio.

4.3.3. Incremental cost-effectiveness ratio

The incremental cost-effectiveness ratio (ICER) is a measure of the additional cost per additional unit of health outcome, and it is used to compare the relative efficiency of different strategies incrementally. When using ICER, an intervention is compared with the next less efficient alternative, and then the next one, until the most cost-efficient intervention is identified. ICER helps to evaluate and compare competing strategies, typically two or more, and make trade-offs between costs and health outcomes.

The ICER is given by,

$$\text{ICER} = \frac{\text{Difference of costs incurred due to intervention strategy j and k}}{\text{Difference in total averted cases in intervention strategy j and k}}.$$

The standard methodology of CEA typically involves four steps: first, defining the problem, the population of interest, and the strategies under consideration; second, estimating the costs and health outcomes associated with each intervention or strategy; third, assessing the cost-effectiveness of each intervention or strategy by comparing ICERs; and interpreting the results and making recommendations.

Defining the problem in cost-effectiveness analysis means identifying the cost of interest in relation to the strategies being evaluated. This includes determining the strategies by making various combinations of inducted controls. In this case, we perform the CEA for the following strategies.

Strategy A: All three controls implemented at a time ($u_1 \neq 0, u_2 \neq 0, u_3 \neq 0$).
Strategy B: Application of only precautionary measures ($u_1 \neq 0, u_2 = 0, u_3 = 0$).
Strategy C: Boosting additional (IDIAS) screening only ($u_1 = 0, u_2 \neq 0, u_3 = 0$).
Strategy D: Boosting treatment only ($u_1 = 0, u_2 = 0, u_3 \neq 0$).
Strategy E: Implementing precautionary measures with boosted screening ($u_1 \neq 0, u_2 \neq 0, u_3 = 0$).
Strategy F: Implementing precautionary measures with boosted treatment ($u_1 \neq 0, u_2 = 0, u_3 \neq 0$).
Strategy G: Boosting both screening and treatment ($u_1 = 0, u_2 \neq 0, u_3 \neq 0$).

Our targeted population of interest includes the individuals who are infectious (with or without symptoms), *i.e.*, a combination of asymptomatic infectious, symptomatic infectious, and infectious individuals under care: $I = I_a + I_s + H$. We use the 'areal approach' to evaluate the numerator and denominator of ICERs. For this population, with respect to each strategy,

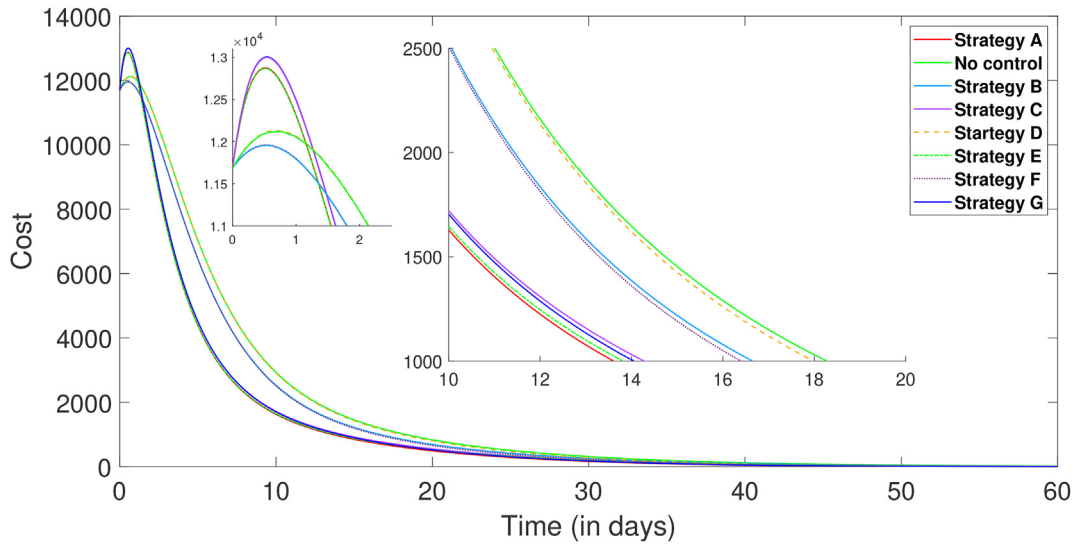

Fig. 30. Illustrating the comparison of costs associated with various strategies, we observe that the green curve, representing the cost incurred by the disease burden in the absence of any control measures, lies below the cost profiles of certain strategies during the initial period when controls are implemented. However, it remains consistently higher than all other cost profiles thereafter. Although the partial overlapping of these cost profiles makes it challenging to directly infer their effectiveness from the curves alone, so we conduct an ICER analysis to better evaluate their cost-effectiveness.

we evaluate the cost incurred (area under the cost profile of $I^*(t)$) and the health outcomes (number of total averted cases), which is nothing but the difference between the area under the curve of $I(t)$ and the curve $I^*(t)$, that is, number of infections without implementation of any control minus the number of infections with a specific strategy of control application. A simple observation tells us that the less the area under the curve $I^*(t)$ more the cases averted; on the other hand, the less the area under the cost profile of the $I^*(t)$, the less cost incurred in averting those much cases. We arrange all the strategies in increasing order of (their health-outcome efficacy) cases averted.

To evaluate the cost incurred, we use the objective cost functional defined in Sub-section 3.2,

$$\mathcal{J}_A = \int_0^{t_f} \left[\underbrace{C_1 I_a(t) + C_2 I_s(t) + C_3 H(t)}_{\text{Cost due to disease prevalence}} + \overbrace{\frac{1}{2}\left(C_4 u_1^2(t) + C_5 u_2^2(t) + C_6 u_3^2(t)\right)}^{\text{Cost of control implementation}} \right] dt, \tag{10}$$

as per the different strategies, for example, the above equation (10) represents the cost of implementing strategy A, while the cost incurred due to the implementation of strategy D would be the combination of cost due to disease prevalence and cost of boosting treatment, that is,

$$\mathcal{J}_D = \int_0^{t_f} \left[C_1 I_a(t) + C_2 I_s(t) + C_3 H(t) + \frac{1}{2}\left(C_6 u_3^2(t)\right) \right] dt.$$

In this way, we plot the cost profilesof different strategies (see Fig. 30) and evaluate the area under the curve of those cost profiles to get the cost of infection aversion and control implementation. The following table has costs and infections averted by the strategies under consideration.

Referring to Table 3, we can infer that a strategy's effectiveness improves with a higher number of averted cases. However, the findings from Table 4 do not permit us to draw a similar conclusion, as the associated costs are also proportionally increasing. At this point, CEA becomes essential in establishing the efficacy ranking of strategies based on their ICERs. We denote the ICER for the jth strategy by $ICER(j)$. We have that strategy A averted the least count of cases, followed by the others. Therefore, ICER for different strategies is evaluated as,

$$ICER(A) = \frac{7.0598 \times 10^7}{5.6489 \times 10^6} = 12.4976$$

$$ICER(E) = \frac{7.1948 \times 10^7 - 7.0598 \times 10^7}{5.8043 \times 10^6 - 5.6489 \times 10^6} = 8.6872$$

$$ICER(G) = \frac{7.2621 \times 10^7 - 7.1948 \times 10^7}{5.8296 \times 10^6 - 5.8043 \times 10^6} = 26.6007$$

$$ICER(C) = \frac{7.3988 \times 10^7 - 7.2621 \times 10^7}{5.9871 \times 10^6 - 5.8296 \times 10^6} = 8.6793$$

$$ICER(F) = \frac{8.8480 \times 10^7 - 7.3988 \times 10^7}{7.4412 \times 10^6 - 5.9871 \times 10^6} = 9.9663$$

$$ICER(B) = \frac{8.9923 \times 10^7 - 8.8480 \times 10^7}{7.6068 \times 10^6 - 7.4412 \times 10^6} = 8.7137$$

$$ICER(D) = \frac{9.6952 \times 10^7 - 8.9923 \times 10^7}{8.2045 \times 10^6 - 7.6068 \times 10^6} = 11.7600$$

Table 3
Strategies in increasing order of their health-outcome efficacy.

Strategy	Cases averted
A	5.6489×10^6
E	5.8043×10^6
G	5.8296×10^6
C	5.9871×10^6
F	7.4412×10^6
B	7.6068×10^6
D	8.2045×10^6

Table 4
Strategies in increasing order of cases averted and cost incurred.

Strategy	Cases averted	Cost incurred
A	5.6489×10^6	7.0598×10^7
E	5.8043×10^6	7.1948×10^7
G	5.8296×10^6	7.2621×10^7
C	5.9871×10^6	7.3988×10^7
F	7.4412×10^6	8.8480×10^7
B	7.6068×10^6	8.9923×10^7
D	8.2045×10^6	9.6952×10^7

Table 5
Listing of strategies with their ICER values and cost-efficacy ranks, among the strategies considered, strategy C (focused on boosting only screening), strategy E (incorporating precautionary measures alongside boosted screening), and strategy B (solely emphasizing precautionary measures) ranked as the top three. However, strategy C is the most cost-effective intervention among all.

Strategy	Cases averted	Cost incurred	ICER	Rank
A	5.6489×10^6	7.0598×10^7	12.4976	Sixth
E	5.8043×10^6	7.1948×10^7	8.6872	**Second**
G	5.8296×10^6	7.2621×10^7	26.6007	Seventh
C	5.9871×10^6	7.3988×10^7	8.6793	**First**
F	7.4412×10^6	8.8480×10^7	9.9663	Fourth
B	7.6068×10^6	8.9923×10^7	8.7137	**Third**
D	8.2045×10^6	9.6952×10^7	11.7600	Fifth

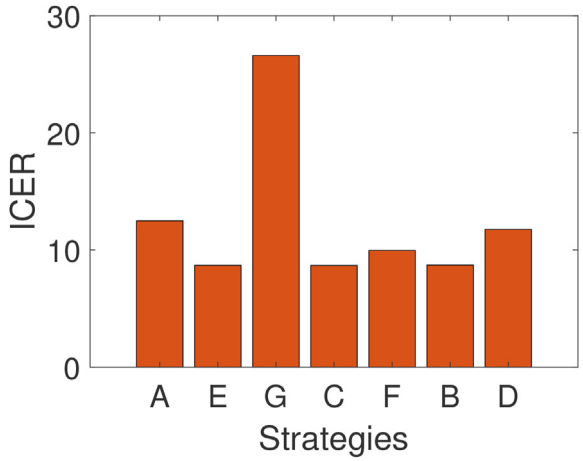

Fig. 31. A bar plot for ICER values of different strategies reveals that strategy G (boosting both screening and treatment) has the highest ICER value indicating its lack of cost-effectiveness. On the other hand, strategy C (boosting only screening) has the lowest ICER value, indicating that this is the most cost-effective intervention.

We determine the cost-efficacy ranks of all strategies based on their ICER, lowest ICER value corresponds to the best strategy because lowest ICER value can only be obtained when increment in cases averted is maximum while keeping the cost incurred at a minimum (see Fig. 31 and Table 5).

The following table has ICER value and the cost-efficacy ranks of the strategies.

This table ascertain that strategy C (only boosting IDIAS) has the lowest ICER value and therefore it is the most cost-effective. However, the difference in ICER values of the strategises C, E, and B is not so distinctive and they stands at the first, second, and third ranks, respectively, but at a larger prospective (more population or highly dense cities) boosting the additional screening is the most cost-effective.

4.4. Summary and public health significance

This sub-section provides a concise overview of the modeling process, data fitting, optimal control analysis and the associated outcomes, emphasizing their public health significance.

4.4.1. Modeling method and process

We established the idea of infectious density-induced additional screening (IDIAS) to examine the feasible efficiency of screening and treatment strategies in reducing the spread of COVID-19. We investigated a *SI2HR* compartmental model that includes saturation treatment as well as non-pharmaceutical controls such as quarantine and screening. The model divides the total population, denoted as N, into five compartments: susceptible individuals (S), asymptomatic infectious individuals (I_a), symptomatic infectious individuals (I_s), infective individuals under care (H), and recovered individuals (R). The population flow among these compartments is described by a set of differential equations. The model incorporates two important rate functions: the screening rate function with infectious density-induced additional screening (IDIAS) and the saturated treatment rate function. The screening rate function, denoted as $\varphi(I_s)$, includes a baseline constant screening (θ) and an additional screening term ($\varphi_1(I_s)$) that depends on the density of infectious individuals. This additional screening, referred to as IDIAS, is crucial for cases where the infectious population varies in density, especially in densely populated areas. The saturated treatment rate function, denoted as $\psi(I_s)$, represents the maximum achievable treatment rate with a saturation effect. This reflects real-world constraints on the number of individuals that can be effectively treated within a given time frame due to resource limitations. The model also considers immunity loss and reinfection dynamics, highlighting their importance in understanding the spread of certain diseases. Recovered individuals can be reinfected at a reduced rate, and immunity loss can lead to individuals moving back to the susceptible compartment.

This *SI2HR* model provides a detailed framework for understanding and simulating the dynamics of disease spread. The inclusion of IDIAS in the screening rate function acknowledges the impact of infectious density on screening efforts, particularly relevant in densely populated areas. Additionally, the saturated treatment rate function reflects practical limitations on the effectiveness of treatment efforts, aligning with real-world constraints in healthcare systems. The consideration of immunity loss and reinfection dynamics adds a crucial layer of realism to the model, making it relevant for diseases where these aspects play a significant role. This modeling approach contributes to the understanding of disease dynamics and can aid public health efforts in planning interventions, resource allocation, and mitigation strategies.

4.4.2. Data fitting and parameter estimation

We validated the formulated model using data fitting and parameter estimation, with a focus on Hong Kong's cases. Through the application of least square technique, the model is fine-tuned to align with the cumulative new infective cases reported between November 1, 2022, and December 29, 2022. The rate equation for cumulative new cases $C(t)$ is fitted to real data, allowing the estimation of key parameters such as the disease transmission rate by symptomatic individuals (β_s) and the additional screening rate (ρ). This validation not only enhances the model's accuracy but also holds significant public health implications, providing a reliable tool for understanding the progression and potentially managing the dynamics of COVID-19 transmission.

The model is then mathematically analyzed to determine the basic reproductive threshold. We discovered disease persistence for $\mathcal{R}_0 > 1$ as well as $\mathcal{R}_0 < 1$ due to saturation treatment. Analytically, we estimated the basic reproduction number, which demonstrates that the number of new infectious cases is sensitive to symptomatic disease transmission rate, baseline screening rate, quarantine/isolation rate and treatment rate. Through sensitivity analysis of the basic reproduction number, we observed that delaying quarantine/self-isolation of asymptomatic individuals results in a massive increase in reproduction.

4.4.3. Optimal control and cost-effectiveness analysis

The mathematical model is further extended to form an optimal control problem (OCP) by incorporating three time-varying control measures, namely, precautionary measures, boosted screening, and boosted treatment. We used numerical techniques (mentioned in 3.2.3) to solve the OCP and simulated the different cases by setting a specific set of parameters and weights. Our objective was to identify the optimal set of controls that simultaneously decreases the disease prevalence and minimizes the costs associated with implementing control measures. We also conducted a comparison of the effectiveness of different combinations of control measures, aiming to identify the intervention or strategy that yields the highest health benefits while incurring the lowest cost. This assessment holds significance for any public health system. Our results demonstrate that the combination of increased screening efforts with precautionary measures or treatment may be beneficial. However, it's important to note that an elevated focus on screening alone can also represent a highly cost-effective strategy as a stand-alone approach. While the adage “precaution is better than cure” holds true, an intermediary approach exists – namely, additional screening at opportune moments – which can prove superior to both preventive measures and treatment.

5. Conclusions

In this article, we proposed and analyzed a novel *SI2HR* model for COVID-19, which incorporates infectious-induced additional screening and treatment saturation. The model was validated using data from Hong Kong, and we established the biological feasibility of our model by proving the positivity and boundedness for the system solutions. Parameter estimation was carried out to determine suitable parameters for the model. we obtained the expression for the reproduction number $\mathcal{R}_0$ corresponding to the infection-free equilibrium, which is locally stable for $\mathcal{R}_0 < 1$ and unstable for $\mathcal{R}_0 > 1$. We also studied the elasticity of $\mathcal{R}_0$, and our analysis showed that the basic reproduction number increases as the disease

transmission rate by symptomatic individuals grows. The negative sensitivity index of parameters γ, α_s, and α demonstrated that an increase in the values of these parameters reduces $\mathcal{R}_0$, indicating the importance of effective screening, quarantine, and treatment measures in controlling the spread of COVID-19. We demonstrated that delaying screening, quarantining, or treating individuals can increase the basic reproduction number of the disease, which indicates the importance of prompt action in controlling the spread of COVID-19. The effective reproductive range is also obtained for all three control measures separately, which shows that boosting additional screening may be helpful in attaining a significant range difference, *i.e.*, lowest value of $\mathcal{R}_0$. We also analyzed the effect of screening on disease spread, and our results showed that additional screening is necessary to control the infection. Specifically, stopping additional screening and baseline screening can increase the number of infective individuals, while providing linear additional screening can decrease the number of infective individuals. This highlights the importance of implementing effective screening measures to control the spread of COVID-19.

In addition to our proposed *SI2HR* model, we extended our analysis by establishing an optimal control problem (OCP) that considers three control measures: precautionary interventions, boosted IDIAS, and boosted treatment. The OCP was solved using Pontryagin's minimum principle and forward-backward sweep method, and numerical simulations showed that boosted screening and treatment with preventive interventions may benefit sustainable disease control. However, we also conducted a cost-effectiveness analysis (CEA) to identify the most cost-effective strategy. Our CEA results suggested that only boosting IDIAS is the most cost-effective strategy among all control measures. We identified specific strategies based on their cost-efficacy rank, which can be implemented to maximize the impact while minimizing costs.

Overall, our analysis not only provides valuable insights into the dynamics of COVID-19 incorporating the effect of infectious-induced additional screening and treatment saturation but also highlights the importance of considering cost-effectiveness in implementing control measures.

Data availability statement

All necessary data for this study are included within the paper and have been properly cited.

CRediT authorship contribution statement

Sonu Lamba: Writing – original draft, Visualization, Validation, Methodology, Investigation, Formal analysis. **Tanuja Das:** Writing – original draft, Visualization, Validation, Methodology, Investigation, Formal analysis. **Prashant K. Srivastava:** Writing – review & editing, Visualization, Supervision, Software, Resources, Methodology, Conceptualization.

Declaration of competing interest

The authors declare that they have no competing interests and have not been involved in any other activities that could be perceived as a potential conflict of interest.

Acknowledgements

SL expresses gratitude to the Ministry of Education, Government of India, for the funding received under the Prime Minister's Research Fellows (PMRF) scheme [PMRF ID: 2701459].

Appendices

A.1 Positive invariability and boundedness (proof of Theorem 3.1)

Proof. From the mathematical model (1), considering that S vanishes at time t_0 before other states become zero, we deduce that at time t_0,

$$\left.\frac{dS}{dt}\right|_{S=0} = \Lambda + \eta R \geq 0,$$

this indicates that S is a non-decreasing time dependent function. Thus, S is non-negative. Following this, similarly, we obtain non-negativity for other state variables also,

$$\left.\frac{dI_a}{dt}\right|_{I_a=0} = \epsilon\beta_s I_s S \geq 0, \left.\frac{dI_s}{dt}\right|_{I_s=0} = (1-\epsilon)\beta_a I_a S + \alpha_a I_a + r\beta_a I_a R \geq 0,$$

$$\left.\frac{dH}{dt}\right|_{H=0} = (\alpha_s I_s + \psi(I_s)) + (\gamma + \varphi(I_s))I_a \geq 0, \left.\frac{dR}{dt}\right|_{R=0} = \sigma H \geq 0.$$

Thus we have established non-negativity for all five states and it is evident that $\mathbb{R}^5_+$ is an invariant set for the model system (1). Besides, the total population $N(= S + E + I_a + I_s + H + R)$ satisfies the differential equation,

$$\frac{dN}{dt} = \Lambda - \mu N,$$

which implies,

$$N(t) = \frac{\Lambda}{\mu}(1 - e^{-\mu t}) + N(0)e^{-\mu t} \leq max\left\{\frac{\Lambda}{\mu} + \left(N(0) - \frac{\Lambda}{\mu}\right)e^{-\mu t}\right\} = \begin{cases} \frac{\Lambda}{\mu} & \text{if } \frac{\Lambda}{\mu} > N(0) \\ N(0) & \text{if } \frac{\Lambda}{\mu} < N(0). \end{cases}$$

If we define a region:

$$\mathcal{D} = \left\{\left(S, I_a, I_s, H, R\right) \in \mathbb{R}^5 : S \geq 0, I_a \geq 0, I_s \geq 0, H \geq 0, R \geq 0, S + E + I_a + I_s + H + R \leq \frac{\Lambda}{\mu}\right\},$$

so for any initial condition from region $\mathcal{D}$, we have $\frac{dS}{dt}\Big|_{S=0} > 0$, $\frac{dI_a}{dt}\Big|_{I_a=0} = 0$, $\frac{dI_s}{dt}\Big|_{I_s=0} = 0$, $\frac{dH}{dt}\Big|_{H=0} = 0$, $\frac{dR}{dt}\Big|_{R=0} = 0$, and also $\frac{dN}{dt}\Big|_{N=\frac{\Lambda}{\mu}} = 0$. Thus, all solutions of system (1) remain inside $\mathcal{D}$ if the initial condition lies in $\mathcal{D}$. Hence, $\mathcal{D}$ is the basic feasible region of system (1).

A.2. Computation of the basic reproduction number

We express the new infection terms and transition terms of system (1) respectively as follows

$$\mathcal{F} = \begin{bmatrix} \epsilon(\beta_s I_s + \beta_a I_a)S \\ (1-\epsilon)(\beta_s I_s + \beta_a I_a)S \end{bmatrix}, \quad \mathcal{V} = \begin{bmatrix} (\gamma + \varphi(I_s))I_a + \alpha_a I_a + \mu I_a \\ -\alpha_a I_a + \alpha_s I_s + \psi(I_s) - r(\beta_s I_s + \beta_a I_a)R + (\mu_s + \mu)I_s \end{bmatrix}$$

Following (Van den Driessche & James, 2002) we get

$$F = \begin{bmatrix} \epsilon\beta_a S_0 & \epsilon\beta_s S_0 \\ (1-\epsilon)\beta_a S_0 & (1-\epsilon)\beta_s S_0 \end{bmatrix}, \quad V = \begin{bmatrix} \gamma + \theta + \alpha_a + \mu & 0 \\ -\alpha_a & \alpha_s + \alpha + \mu_s + \mu \end{bmatrix}.$$

Which implies,

$$FV^{-1} = \begin{bmatrix} \epsilon\dfrac{\beta_a S_0}{\gamma + \theta + \alpha_a + \mu} + \dfrac{\epsilon\alpha_a\beta_s S_0}{(\gamma + \theta + \alpha_a + \mu)(\alpha_s + \alpha + \mu_s + \mu)} & \dfrac{\epsilon\beta_s S_0}{\alpha_s + \alpha + \mu_s + \mu} \\ (1-\epsilon)\dfrac{\beta_a S_0}{\gamma + \theta + \alpha_a + \mu} + \dfrac{(1-\epsilon)\alpha_a\beta_s S_0}{(\gamma + \theta + \alpha_a + \mu)(\alpha_s + \alpha + \mu_s + \mu)} & \dfrac{(1-\epsilon)\beta_s S_0}{\alpha_s + \alpha + \mu_s + \mu} \end{bmatrix},$$

and the spectral radius of the matrix FV^{-1} is as follows

$$\mathcal{R}_0 = \rho(FV^{-1}) = \epsilon\frac{\beta_a S_0}{(\gamma + \theta + \alpha_a + \mu)} + \epsilon\frac{\alpha_a}{(\gamma + \theta + \alpha_a + \mu)}\frac{\beta_s S_0}{(\alpha_s + \alpha + \mu_s + \mu)} + \frac{(1-\epsilon)\beta_s S_0}{(\alpha_s + \alpha + \mu_s + \mu)}.$$

A.3. Local stability of IFE (proof of Theorem 3.2)

The Jacobian matrix at IFE E_1 is given by

$$J|_{E_1} = \begin{bmatrix} d_{11} & d_{12} & d_{13} & 0 & d_{15} \\ 0 & d_{22} & d_{23} & 0 & 0 \\ 0 & d_{32} & d_{33} & 0 & 0 \\ 0 & d_{42} & d_{43} & d_{44} & 0 \\ 0 & 0 & 0 & d_{54} & d_{55} \end{bmatrix}, \tag{11}$$

where, $d_{11} = -\mu$, $d_{12} = -\beta_a S_0$, $d_{13} = -\beta_s S_0$, $d_{15} = \eta$, $d_{22} = \epsilon\beta_a S_0 - (\gamma + \theta + \alpha_a + \mu)$, $d_{23} = \epsilon\beta_s S_0$, $d_{32} = (1-\epsilon)\beta_a S_0 + \alpha_a$, $d_{33} = (1-\epsilon)\beta_s S_0 - (\alpha_s + \alpha + \mu_s + \mu)$, $d_{42} = \gamma + \theta$, $d_{43} = \alpha_s + \alpha$, $d_{44} = -(\sigma + \mu)$, $d_{54} = \sigma$, $d_{55} = -(\eta + \mu)$.

The corresponding characteristic equation is,

$$(\lambda - d_{11})(\lambda - d_{44})(\lambda - d_{55})(\lambda^2 - (d_{22} + d_{33})\lambda + (\gamma + \theta + \alpha_a + \mu)(\alpha_s + \alpha + \mu_s + \mu)(1 - \mathcal{R}_0)) = 0. \tag{12}$$

As $\mathcal{R}_0 < 1$ implies that $d_{22} < 0$ and $d_{33} < 0$, so all roots of characteristic equation (12) are negative when $\mathcal{R}_0 < 1$. One root of characteristic equation (12) is positive when $\mathcal{R}_0 > 1$. Hence, the IFE E_1 is locally stable for $\mathcal{R}_0 < 1$ and unstable for $\mathcal{R}_0 > 1$.

A.4. Bifurcation at $\mathcal{R}_0 = 1$ (proof of Theorem 3.3)

It is noted that the matrix $J|_{E_1}$ in (11) has one zero eigenvalue and remains all negative at $\mathcal{R}_0 = 1$. Also, $\mathcal{R}_0 = 1$ gives $\mu = \mu^* :=$. In order to study the occurrence of bifurcations at (E_1, β_s^*) we follow the Sotomayor theorem (Lawrence, 2013) and perform the below computation:

$$\begin{aligned}
\Delta_1 &= Y^T[0,0,0,0,0]^T = 0,\\
\Delta_2 &= Y^T \begin{bmatrix} 0 & 0 & -S_0 & 0 & 0 \\ 0 & 0 & -\epsilon S_0 & 0 & 0 \\ 0 & 0 & -(1-\epsilon)S_0 & 0 & 0 \\ 0 & 0 & 0 & 0 & 0 \\ 0 & 0 & 0 & 0 & 0 \end{bmatrix} X = [0,0,-\epsilon S_0 y_2 - (1-\epsilon)S_0, 0, 0]X = -x_3(\epsilon S_0 y_2 + (1-\epsilon)S_0),\\
\Delta_3 &= 2Y^T \left(\begin{bmatrix} -\beta_a \\ \epsilon\beta_a \\ (1-\epsilon)\beta_a \\ 0 \\ 0 \end{bmatrix} x_1x_2 + \begin{bmatrix} -\beta_s \\ \epsilon\beta_s \\ (1-\epsilon)\beta_s \\ 0 \\ 0 \end{bmatrix} x_1x_3 + \begin{bmatrix} 0 \\ -\rho \\ 0 \\ \rho \\ 0 \end{bmatrix} x_2x_3 + \begin{bmatrix} 0 \\ 0 \\ r\beta_a \\ 0 \\ -r\beta_a \end{bmatrix} x_2x_5 + \begin{bmatrix} 0 \\ 0 \\ r\beta_s \\ 0 \\ -r\beta_s \end{bmatrix} x_3x_5 + \begin{bmatrix} 0 \\ 0 \\ -\alpha\nu \\ \alpha\nu \\ 0 \end{bmatrix} x_3^2 \right),\\
&= 2((\epsilon\beta_a y_2 + (1-\epsilon)\beta_a)x_1 + (\epsilon\beta_s y_2 + (1-\epsilon)\beta_s)x_1x_3 - \rho x_3 y_2 + \rho\beta_a x_5 + \rho\beta_s x_3 x_5 - \alpha\nu x_3^2),
\end{aligned}$$

where, $X := [x_1, x_2, x_3, x_4, x_5]^T = [-\frac{(d_{12}d_{23} - d_{13}d_{22})d_{44}d_{55} + d_{15}d_{54}(d_{42}d_{23} - d_{43}d_{22})}{d_{11}d_{44}d_{55}d_{23}}, 1, -\frac{d_{22}}{d_{23}}, \frac{d_{43}d_{22} - d_{42}d_{23}}{d_{23}d_{44}}, \frac{d_{54}(d_{42}d_{23} - d_{43}d_{22})}{d_{23}d_{44}d_{55}}]^T$ and $Y = [y_1, y_2, y_3, y_4, y_5]^T = [0, -\frac{d_{32}}{d_{22}}, 1, 0, 0]^T$, respectively are the right and left eigenvectors of $J|_{E_1}$ with respect to zero eigenvalue. Since $d_{22} < 0$, $d_{23} > 0$ and $d_{32} > 0$ for $\mathcal{R}_0 = 1$, x_3 and y_2 are positive. Hence, Δ_2 is positive. However, Δ_3 is positive if $\nu < \nu_{crit} := \frac{(\epsilon\beta_a y_2 + (1-\epsilon)\beta_a)x_1 + (\epsilon\beta_s y_2 + (1-\epsilon)\beta_s)x_1x_3 - \rho x_3 y_2 + \rho\beta_a x_5 + \rho\beta_s x_3 x_5}{\alpha x_3^2}$ and negative if $\nu > \nu_{crit}$.

A.5. Local stability of endemic equilibrium (proof of Theorem 3.4)

The Jacobian matrix at endemic equilibrium E_2^* is given by

$$J|_{E_2^*} = \begin{bmatrix} a_{11} & a_{12} & a_{13} & 0 & a_{15} \\ a_{21} & a_{22} & a_{23} & 0 & 0 \\ a_{31} & a_{32} & a_{33} & 0 & a_{35} \\ 0 & a_{42} & a_{43} & a_{44} & 0 \\ 0 & a_{52} & a_{53} & a_{54} & a_{55} \end{bmatrix},$$

where, $a_{11} = -(\beta_s I_s^* + \beta_a I_a^* + \mu)$, $a_{12} = -\beta_a S^*$, $a_{13} = -\beta_s S^*$, $a_{15} = \eta$, $a_{21} = \epsilon(\beta_s I_s^* + \beta_a I_a^*)$, $a_{22} = \epsilon\beta_a S^* - (\gamma + \theta + \frac{\rho I_s^*}{1+mI_s^*} + \alpha_a + \mu)$, $a_{23} = \epsilon\beta_s S^* - \frac{\rho I_a^*}{(1+mI_s^*)^2}$, $a_{31} = (1-\epsilon)(\beta_s I_s^* + \beta_a I_a^*)$, $a_{32} = (1-\epsilon)\beta_a S^* + \alpha_a + r\beta_a R^*$, $a_{33} = (1-\epsilon)\beta_s S^* - (\alpha_s + \frac{\alpha}{(1+\nu I_s^*)^2} + \mu + \mu_s) + r\beta_s R^*$, $a_{35} = r(\beta_s I_s^* + \beta_a I_a^*)$, $a_{42} = \gamma + \theta + \frac{\rho I_s^*}{1+mI_s^*}$, $a_{43} = \alpha_s + \frac{\alpha}{(1+\nu I_s^*)^2} + \frac{\rho I_a^*}{(1+mI_s^*)^2}$, $a_{44} = -(\sigma + \mu)$, $a_{52} = -r\beta_a R^*$, $a_{53} = -r\beta_s R^*$, $a_{54} = \sigma$, $a_{55} = -r(\beta_s I_s^* + \beta_a I_a^*) - (\eta + \mu)$.

The corresponding characteristic equation is,

$$\lambda^5 + b_4\lambda^4 + b_3\lambda^3 + b_2\lambda^2 + b_1\lambda + b_0 = 0, \tag{13}$$

where,

$$
\begin{aligned}
b_4 = {} & -a_{11}-a_{22}-a_{33}-a_{44}-a_{55},\\
b_3 = {} & a_{11}a_{22}-a_{12}a_{21}+a_{11}a_{33}-a_{13}a_{31}+a_{11}a_{44}+a_{22}a_{33}-a_{23}a_{32}+a_{11}a_{55}+a_{22}a_{44}+a_{22}a_{55}+a_{33}a_{44}+\\
& a_{33}a_{55}-a_{35}a_{53}+a_{44}a_{55}\\
b_2 = {} & a_{11}a_{23}a_{32}-a_{11}a_{22}a_{33}+a_{12}a_{21}a_{33}-a_{12}a_{23}a_{31}-a_{13}a_{21}a_{32}+a_{13}a_{22}a_{31}-a_{11}a_{22}a_{44}+a_{12}a_{21}a_{44}-a_{11}a_{22}a_{55}\\
& -a_{11}a_{33}a_{44}+a_{12}a_{21}a_{55}+a_{13}a_{31}a_{44}-a_{15}a_{21}a_{52}-a_{11}a_{33}a_{55}+a_{11}a_{35}a_{53}+a_{13}a_{31}a_{55}-a_{15}a_{31}a_{53}-a_{22}a_{33}\\
& a_{44}+a_{23}a_{32}a_{44}-a_{11}a_{44}a_{55}-a_{22}a_{33}a_{55}+a_{22}a_{35}a_{53}+a_{23}a_{32}a_{55}-a_{23}a_{35}a_{52}-a_{22}a_{44}a_{55}-a_{33}a_{44}a_{55}-\\
& a_{35}a_{43}a_{54}+a_{35}a_{44}a_{53},\\
b_1 = {} & a_{11}a_{22}a_{33}a_{44}-a_{11}a_{23}a_{32}a_{44}-a_{12}a_{21}a_{33}a_{44}+a_{12}a_{23}a_{31}a_{44}+a_{13}a_{21}a_{32}a_{44}-a_{13}a_{22}a_{31}a_{44}+a_{11}a_{22}a_{33}a_{55}-\\
& a_{11}a_{22}a_{35}a_{53}-a_{11}a_{23}a_{32}a_{55}+a_{11}a_{23}a_{35}a_{52}-a_{12}a_{21}a_{33}a_{55}+a_{12}a_{21}a_{35}a_{53}+a_{12}a_{23}a_{31}a_{55}+a_{13}a_{21}a_{32}a_{55}-\\
& a_{13}a_{21}a_{35}a_{52}-a_{13}a_{22}a_{31}a_{55}-a_{15}a_{21}a_{32}a_{53}+a_{15}a_{21}a_{33}a_{52}+a_{15}a_{22}a_{31}a_{53}-a_{15}a_{23}a_{31}a_{52}+a_{11}a_{22}a_{44}a_{55}-\\
& a_{12}a_{21}a_{44}a_{55}-a_{15}a_{21}a_{42}a_{54}+a_{15}a_{21}a_{44}a_{52}+a_{11}a_{33}a_{44}a_{55}+a_{11}a_{35}a_{43}a_{54}-a_{11}a_{35}a_{44}a_{53}-a_{13}a_{31}a_{44}a_{55}-\\
& a_{15}a_{31}a_{43}a_{54}+a_{15}a_{31}a_{44}a_{53}+a_{22}a_{33}a_{44}a_{55}+a_{22}a_{35}a_{43}a_{54}-a_{22}a_{35}a_{44}a_{53}-a_{23}a_{32}a_{44}a_{55}-a_{23}a_{35}a_{42}a_{54}+\\
& a_{23}a_{35}a_{44}a_{52},\\
b_0 = {} & a_{11}a_{22}a_{35}a_{44}a_{53}-a_{11}a_{22}a_{33}a_{44}a_{55}-a_{11}a_{22}a_{35}a_{43}a_{54}+a_{11}a_{23}a_{32}a_{44}a_{55}+a_{11}a_{23}a_{35}a_{42}a_{54}-a_{11}a_{23}a_{35}a_{44}a_{52}+\\
& a_{12}a_{21}a_{33}a_{44}a_{55}+a_{12}a_{21}a_{35}a_{43}a_{54}-a_{12}a_{21}a_{35}a_{44}a_{53}-a_{12}a_{23}a_{31}a_{44}a_{55}-a_{13}a_{21}a_{32}a_{44}a_{55}-a_{13}a_{21}a_{35}a_{42}a_{54}+\\
& a_{13}a_{21}a_{35}a_{44}a_{52}+a_{13}a_{22}a_{31}a_{44}a_{55}-a_{15}a_{21}a_{32}a_{43}a_{54}+a_{15}a_{21}a_{32}a_{44}a_{53}+a_{15}a_{21}a_{33}a_{42}a_{54}-a_{15}a_{21}a_{33}a_{44}a_{52}+\\
& a_{15}a_{22}a_{31}a_{43}a_{54}-a_{15}a_{22}a_{31}a_{44}a_{53}-a_{15}a_{23}a_{31}a_{42}a_{54}+a_{15}a_{23}a_{31}a_{44}a_{52}.
\end{aligned}
\tag{14}
$$

We get the Routh array:

$$
\begin{array}{ccc}
1 & b_3 & b_1\\
b_4 & b_2 & b_0\\
a^* & b^* & 0\\
c^* & b_0 & 0\\
d^* & 0 & 0\\
b_0 & 0 & 0
\end{array}
$$

where, $a^* = \frac{b_4b_3-b_2}{b_4}$, $b^* = \frac{b_4b_1-b_0}{b_4}$, $c^* = \frac{b_2a^*-b_4b^*}{a^*}$, and $d^* = \frac{c^*b^*-b_0a^*}{c^*}$. So by Routh-Hurwitz criterion, all roots of equation (13) will be negative if $b_0>0$, $b_4>0$, $b_4b_3-b_2>0$, $b_2(b_4b_3-b_2)-b_4(b_4b_1-b_0)>0$, and $(b_2(b_4b_3-b_2)-b_4(b_4b_1-b_0))(b_4b_1-b_0)-b_0(b_4b_3-b_2)^2>0$.

References

Agusto, F. B., & Elmojtaba, I. M. (2017). Optimal control and cost-effective analysis of malaria/visceral leishmaniasis co-infection. *PLoS One, 12*(2), Article e0171102.

Aldila, D., Meksianis, Z., Ndii, Brenda, M., & Samiadji. (2020). Optimal control on covid-19 eradication program in Indonesia under the effect of community awareness. *Mathematical Biosciences and Engineering, 17*(6), 6355–6389.

Aleta, A., Martin-Corral, D., Pastore y Piontti, A., Ajelli, M., Litvinova, M., Chinazzi, M., … Pentland, A. (2020). Modelling the impact of testing, contact tracing and household quarantine on second waves of COVID-19. *Nature Human Behaviour, 4*(9), 964–971.

Andermann, A., Blancquaert, I., Beauchamp, S., & Déry, V. (2008). Revisiting wilson and jungner in the genomic age: A review of screening criteria over the past 40 years. *Bulletin of the World Health Organization, 86*(4), 317–319.

Bonyah, E., Khan, M. A., Ko, O., & Islam, S. (2017). A theoretical model for zika virus transmission. *PLoS One, 12*(10), Article e0185540.

Cristiane, M., Batistela, Correa, D. P. F., Átila, M., Bueno, & C Piqueira, J. R. (2021). Sirsi compartmental model for covid-19 pandemic with immunity loss. *Chaos, Solitons & Fractals, 142*, Article 110388.

Das, T., Ramdas Bandekar, S., Kumar Srivastav, A., Prashant, K., Srivastava, & Ghosh, M. (2023). Role of immigration and emigration on the spread of COVID-19 in a multipatch environment: A case study of India. *Scientific Reports, 13*(1), 1054.

de Meijere, G., Valdano, E., Castellano, C., Debin, M., Kengne-Kuetche, C., Turbelin, C., … Hens, N. (2023). Attitudes towards booster, testing and isolation, and their impact on COVID-19 response in winter 2022/2023 in France, Belgium, and Italy: A cross-sectional survey and modelling study. *The Lancet Regional Health–Europe, 28*.

Gaff, H., & Schaefer, E. (2009). Optimal control applied to vaccination and treatment strategies for various epidemiological models. *Mathematical Biosciences and Engineering, 6*(3), 469.

Gao, S., Binod, P., Chukwu, C. W., Kwofie, T., Safdar, S., Newman, L., … van den Driessche, P. (2023). A mathematical model to assess the impact of testing and isolation compliance on the transmission of COVID-19. *Infectious Disease Modelling, 8*(2), 427–444.

Gold, M. R., Siegel, J. E., Rusell, L. B., & Weinstein, M. C. (1996). Cost-effectiveness in health and medicine. *Cost-effectiveness in health and medicine*, 425–425.

Hsieh, Y.-H. (1991). Modelling the effects of screening in hiv transmission dynamics. In *Differential equations models in biology, epidemiology and ecology* (pp. 99–120). Springer.

Kim, M. Y., & Milner, F. A. (1995). A mathematical model of epidemics with screening and variable infectivity. *Mathematical and Computer Modelling, 21*(7), 29–42.

Kumar, A., Prashant, K., & Srivastava. (2017). Vaccination and treatment as control interventions in an infectious disease model with their cost optimization. *Communications in Nonlinear Science and Numerical Simulation, 44*, 334–343.

Kumar, A., Prashant, K., Srivastava, & Takeuchi, Y. (2017). Modeling the role of information and limited optimal treatment on disease prevalence. *Journal of Theoretical Biology, 414*, 103–119.

Lamba, S., Prashant, K., & Srivastava. (2023). Cost-effective optimal control analysis of a covid-19 transmission model incorporating community awareness and waning immunity. *Computational and Mathematical Biophysics, 11*(1), Article 20230154.

Lawrence, P. (2013). *Differential equations and dynamical systems, ume 7*. Springer Science & Business Media.
Lenhart, S., & Workman, J. T. (2007). *Optimal control applied to biological models*. Chapman and Hall/CRC.
Li, R., Pei, S., Chen, B., Song, Y., Zhang, T., Yang, W., & Shaman, J. (2020). Substantial undocumented infection facilitates the rapid dissemination of novel coronavirus (sars-cov-2). *Science, 368*(6490), 489–493.
Lin, J., Huang, W., Wen, M., Li, D., Ma, S., Hua, J., Hu, H., Yin, S., Qian, Y., Chen, P., & Zhang, Q. (2020). Containing the spread of coronavirus disease 2019 (COVID-19): Meteorological factors and control strategies. *Science of the Total Environment, 744*, 140935.
Maxwell Glover Wilson, J., & Jungner, G. (1968). *Principles and practice of screening for disease*. Public Health Papers by World Health Organization.
Rami, H., Al-Rifai, Juan Acuna, Ismail Al Hossany, F., Aden, B., & Ahmed, L. A. (2021). Epidemiological characterization of symptomatic and asymptomatic covid-19 cases and positivity in subsequent rt-pcr tests in the United Arab Emirates. *PLoS One, 16*(2), Article e0246903.
Robert Mccredie May and Roy Malcolm Anderson. (1988). The transmission dynamics of human immunodeficiency virus (hiv). *Philosophical Transactions of the Royal Society of London B Biological Sciences, 321*, 565–607.
Saha, P., Sudhanshu Kumar Biswas, M. H. A., Biswas, & Ghosh, U. (2023). An seqaihr model to study covid-19 transmission and optimal control strategies in Hong Kong, 2022. *Nonlinear Dynamics, 111*(7), 6873–6893.
Srivastav, A., Kumar Tiwari, P., Prashant, K., Srivastava, Ghosh, M., & Kang, Y. (2021). A mathematical model for the impacts of face mask, hospitalization and quarantine on the dynamics of covid-19 in India: Deterministic vs. stochastic. *Mathematical Biosciences and Engineering, 18*(1), 182–213.
Srivastava, A., Sonu, Prashant, K., & Srivastava. (2022). Nonlinear dynamics of a siri model incorporating the impact of information and saturated treatment with optimal control. *The European Physical Journal Plus, 137*(9), 1–25.
Sun, C., Yang, W., Arino, J., & Khan, K. (2011). Effect of media-induced social distancing on disease transmission in a two patch setting. *Mathematical Biosciences, 230*(2), 87–95.
URL. https://www.worldometers.info/coronavirus/country/china-hong-kong-sar/.
Van den Driessche, P., & James, W. (2002). Reproduction numbers and sub-threshold endemic equilibria for compartmental models of disease transmission. *Mathematical Biosciences, 180*(1–2), 29–48.
Wald, N. J., Hackshaw, A. K., & Frost, C. D. (1999). When can a risk factor be used as a worthwhile screening test? *British Medical Journal, 319*(7224), 1562–1565.
Wendell, H., Fleming, & Rishel, R. W. (2012). *Deterministic and stochastic optimal control, ume 1*. Springer Science & Business Media.
Xue, L., Jing, S., & Wang, H. (2021). Evaluating the impacts of non-pharmaceutical interventions on the transmission dynamics of covid-19 in Canada based on mobile network. *PLoS One, 16*(12), Article e0261424.
Yuan, H.-Y., & Blakemore, C. (2022a). The impact of contact tracing and testing on controlling covid-19 outbreak without lockdown in Hong Kong: An observational study. *The Lancet Regional Health-Western Pacific, 20*, Article 100374.
Yuan, H.-Y., & Blakemore, C. (2022b). The impact of multiple non-pharmaceutical interventions on controlling covid-19 outbreak without lockdown in Hong Kong: A modelling study. *The Lancet Regional Health-Western Pacific, 20*, Article 100343.
Zhang, N., Chan, P. T. J., Jia, W., Dung, C. H., Zhao, P., Lei, H., … Li, Y. (2021). Analysis of efficacy of intervention strategies for COVID-19 transmission: A case study of Hong Kong. *Environment International, 156*, 106723.